PNAS
www.pnas.org

Supplementary Information for
Galectin-3 N-terminal tail prolines modulate cell activity and glycan-mediated oligomerization/phase separation

Zihan Zhao[a], Xuejiao Xu[a], Hairong Cheng[a], Michelle C. Miller[b], Zhen He[a], Hongming Gu[a], Zhongyu Zhang[a], Avraham Raz[c], Kevin H. Mayo[b], Guihua Tai[a,1], and Yifa Zhou[a,1]

[1]Correspondence: taigh477@nenu.edu.cn (GT), zhouyf383@nenu.edu.cn (YZ)

This PDF file includes:

Supplementary results

Gal-3 LLPS induced by high salt. We performed LLPS experiments with Gal-3 in high salt and found that droplet formation was dependent on the concentrations of both Gal-3 (≥10 μM) and NaCl (≥1.0 M) (*SI Appendix*, Fig. S4 *A* and *B*). Because droplets formed at 37°C but not at 4°C (*SI Appendix*, Fig. S4*C*), it appears that molecular interactions are mediated by hydrophobic forces. Using NT-truncated Gal-3 variants (*SI Appendix*, Fig. S4*D*), we found that deletion of the first 12 NT residues did not affect droplet formation, whereas deletion of the first 68 NT residues or all NT residues (i.e., truncated CRD) abolished it (*SI Appendix*, Fig. S4 *B* and *E*). Moreover, although NT peptide residues 1 to 108 promote droplet formation, full-length Gal-3 requires a higher salt concentration than the NT alone (*SI Appendix*, Fig. S4*B*). This suggests that the presence of the CRD tends to attenuate high salt-mediated LLPS, with NT–NT hydrophobic interactions likely providing the driving force for droplet formation. Supporting this conclusion, we find that neither the S-face glycan binding site R186S mutation nor the F-face L203A mutation affect droplet formation (*SI Appendix*, Fig. S4*F*).

Gal-3 NT–CRD exchange dynamics assessed by NMR spectroscopy. We compared the ^{15}N-HSQC spectra of wild-type (WT) Gal-3 and Gal-3 NT proline mutants as exemplified in *SI Appendix*, Fig. S9*A* with the NT mutant P46A and analysed changes in the chemical shifts (Δδ) and resonance broadening (ΔINT). Δδ values reflect environmental/conformational changes, and ΔINT values reflect changes in exchange dynamics and/or internal motions. Even though the new residue A46 induces the anticipated relatively large chemical shift changes at sequentially neighbouring residues Y45 and G47, other significant chemical shift changes, albeit smaller, are observed throughout the lectin (*SI Appendix*, Fig. S9*B*), in particular within the NT and CRD F-face, as highlighted on the structure of the Gal-3 CRD (PDB 1A3K, *SI Appendix*, Fig. S9*C*). Furthermore, ^{1}H Δδ values for P46A F-face residues (full-length Gal-3 vs. Gal-3 CRD) correlate well (R^2 = 0.71) with those of WT Gal-3 (full-length Gal-3 vs. Gal-3 CRD) (*SI Appendix*, Fig. S9*D*), indicating that the NT in both cases interacts with essentially the same set of F-face residues. The mutation of a single proline (P46) can induce such significant effects throughout the lectin, especially considering that P46 is located within the highly dynamic, aperiodic NT.

More informative, however, is that ΔINT values for most NT residues between 40 and 60 and CRD residues 200 to 220 are positive, indicating increased resonance broadening and thus somewhat stronger NT–CRD interactions between these segments in P46A compared to those in WT Gal-3 (*SI Appendix*, Fig. S9*E*). It is also notable that most other

residues throughout P46A exhibit greater mobility (i.e., negative ΔINT values, *SI Appendix*, Fig. S9*E*), especially those within the sugar binding CRD S-face, e.g., residues 130 to 190 (*SI Appendix*, Fig. S9*E*). Other Gal-3 NT proline mutants show similar effects, with ΔINT and Δδ values varying throughout the lectin (*SI Appendix*, Fig. S9 *F* and *G*). Differential effects are exemplified by ΔINT values through NT residues for all mutants shown in *SI Appendix*, Fig. S9*F*. Depending on the particular NT mutant, not all resonances could be unambiguously assigned, such that the absence of a change does not necessarily indicate anything. Nevertheless, some NT mutants show regions of increased or decreased resonance broadening suggestive of stronger or weaker interactions, respectively, with the CRD F-face. *SI Appendix*, Table S2 shows CRD and NT sequence-averaged Δδ and ΔINT values for each NT proline mutant. Compared to WT Gal-3, the average Δδ values vary from ~0.01 ppm (~8.5 Hz) up to ~0.06 ppm (~50 Hz), and the average ΔINT values range from -0.36 to +0.09. Although NT–CRD interactions and exchange dynamics vary considerably over NT mutants, one interpretation of negative ΔINT values is greater mobility and solvent exposure of the NT, whereas more positive values suggest reduced NT mobility and somewhat less solvent exposure.

Supplementary Materials and Methods

Materials and reagents. Glycoproteins CD45 (16884-H08H), CD71 (11020-H07H), and CD7 (11028-H08H) were purchased from Sino Biological (Beijing, China). Anti-CD146 (sc-18837) was purchased from Santa Cruz Biotechnology (Santa Cruz, CA, USA). Anti–Gal-3 or anti-NT (87985) to identify residues near the N-terminus of Gal-3 was purchased from Cell Signal Technology (Beverly, MA, USA). Anti-His (KM8001) was purchased from Sungene Biotech (Beijing, China). Actin (612657) and FITC mouse anti-human CD69 (555530) were purchased from BD Biosciences (San Jose, CA, USA). Human IL-2 ELISA Kit (EK0397) was purchased from Boster Biological Technology Co., Ltd. (Wuhan, China). LLOMe (L7393) was purchased from Sigma-Aldrich (St. Louis, MO, USA). The protease inhibitor cocktail was purchased from Bimake (Shanghai, China). Eight peptides, pep21 (sequence: GWPGAWGN), pep28 (sequence: NQPAGAGG), pep35 (sequence: GYPGASYP), pep40 (sequence: SYPGAYPG), pep44 (sequence: AYPGQAPP), pep51 (sequence: PGAYPGQA), pep57 (sequence: QAPPGAYP), and pep62 (sequence: AYPGAPGA) were commercially synthesized by GL Biochem (Shanghai, China) with purity >98%. Lactose (Lac, purity 99%, Shanghai Yuanye Bio-Technology, China), N-Acetyl-D-Lactosamine (LacNAc, purity 98%, aladdin, China), and Tri-N-Acetyl-D-Lactosamine [$(LacNAc)_3$, purity >85%, ELICITYL, France] were purchased from respective companies.

Protein expression and purification. Recombinant human Gal-1, Gal-2, Gal-3, and Gal-3 truncates were prepared as previously reported (1, 2). Recombinant proteins were obtained using a PET28a or PET22b vector (Novagen, Gibbstown, NJ, USA). *E. coli* BL21 were induced to express protein by incubating with 0.5 μM IPTG for 16 h at 25°C and purified using nickel beads (Qiagen, GmbH, Hilden, Germany) according to the manufacturer's instructions or Lactose-Sepharose CL-6B beads according to previously reported protocol (1). Purity was analysed by SDS-PAGE.

Gal-3 NT proline mutants (P17A, P19A, P23A, P30A, P37A, P42A, P46A, P50A, P51A, P55A, P59A, P60A, P64A, P67A, and P64H) and L203A were obtained by mutating the plasmid (performed by Synbio Technologies, China), transferring the mutated plasmid into *E. coli* BL21, and then preparing proteins according to the above described method. The Gal-3(R186S) mutant was obtained by mutating Gal-3 in the PET3c plasmid (performed by Synbio Technologies, China), transferring the plasmid into *E. coli* BL21, and then preparing proteins as previously reported (3). To express GFP-fused proteins, the GFP gene was fused to the 5' end of target genes (done by Synbio Technologies, China), transferring the fused plasmid into *E. coli* BL21, and then preparing proteins according to the above described method.

CD146 and CD146 D1 to D4 were prepared as previously reported (4). All the purified proteins were divided into aliquots and stored at -80°C. PNGase F-treated CD146 was prepared by incubating 2 μM CD146 with 1000 U PNGase F at 37°C for 1 h using a PNGase F Kit (P0704S, NEW ENGLAND BioLabs) according to the manufacturer's instructions.

Cell culture. The human leukemic T cell line Jurkat (ATCC TIB-152, USA) was maintained at 37°C and 5% CO_2 in RPMI 1640 medium (Gibco, NY, USA) supplemented with 10% FCS (Gibco, NY, USA) and 1% penicillin-streptomycin (PAN Biotech, Aidenbach, Germany). Human microvascular endothelial cell (HMEC-1) was purchased from the American Type Culture Collection (ATCC CRL-3243, USA) and maintained in MCDB131 medium (Gibco, NY, USA) supplemented with 10% FCS, 10 mM L-glutamine (Sigma, St. Louis, MO, USA), 10 ng/ml recombinant EGF, 1 μg/ml hydrocortisone (Sigma, St. Louis, MO, USA) and 1% penicillin-streptomycin. Human embryonic kidney (HEK) 293T cells were obtained from the Cell Bank of the Chinese Academy of Sciences (Shanghai, China) and maintained in DMEM (Gibco, NY, USA) with 10% FCS and 1% penicillin-streptomycin.

Endothelial cell migration. Real-time measurements of cell migration were performed using a xCELLigence RTCA DP (real-time cell analyzer dual purpose) instrument and CIM-plates from Roche Diagnostics (Mannheim, Germany). CIM-plates are similar to a Boyden chamber, in that it contains an upper and a lower chamber separated by a polyethylene terephthalate membrane (8 μm pore size). The membrane has gold electrodes on the bottom of the upper chamber to detect cells moving into the lower chamber. Migration rates were quantitatively recorded as the Cell Index (change in electrical impedance of current flowing through the electrodes). For this purpose, the HMEC-1 cells were digested with trypsin and resuspended in serum-free MCDB131 medium. Then, 5 x 10^4 cells were seeded per well in the upper chamber of a CIM plate. This upper chamber was then placed on the lower part of the plate containing serum-free MCDB131 medium supplemented with 0.7 μM wild-type Gal-3 or mutants as an attractant or without Gal-3 (negative control). In some cases, 4 mM Lac or sucrose (Suc) was added. The assay was performed as detailed by Roche Diagnostics in the instruction manual. Cell migration (represented by Cell Index) was followed over a time period of up to 18 h by changes in the impedance signal in a CIM-plate measured on the backside of the membrane as described for the xCELLigence DP system. Data acquisition and analysis were performed with RTCA software (version 1.2, Roche Diagnostics). The Cell Index values at 4 h, 7 h, and 10 h were analysed statistically (Fig. 1*A*).

T-cell activation assays. Jurkat cells (2 x 10^6 cells/well) in serum-free medium were seeded into 12-well plates and cocultured with 1.0 μM wild-type Gal-3 or mutants for 6 h (for analysis of CD69 expression) or 18 h (for analysis of IL-2 expression), followed by centrifugation to separate the cell pellets and the supernatant. In some cases, 4 mM Lac or Suc or 5 mM octapeptides was included in the coculture. To determine CD69 expression, the cells were washed once with PBS and incubated on ice with FITC-conjugated anti-CD69 antibody for 30 min in the dark. Following extensive washing with cold PBS, the cells were measured by BD Accuri™ C6 (488 nm excitation and 530 nm emission). To determine IL-2 expression, the supernatant was tested using the Human IL-2 ELISA Kit (Boster Biological Technology Co., Ltd.) according to the manufacturer's protocol. Briefly, 100 μl of the supernatant was added to an ELISA plate. After incubation with the primary antibody and the secondary antibody and colour development, the absorbance at 450 nm was measured with a microplate reader.

Hemagglutination assays. This assay was performed as previously described (5). Each well of a microtiter V plate contained 50 μl of PBS, 25 μl of increasing concentrations of wild-type Gal-3 or mutants, and 25 μl of a 4% (V/V) chicken erythrocyte or human erythrocyte suspension. In some cases, 4 mM Lac was added. All dilutions were performed in PBS. Agglutination was allowed to proceed for 60 min at 4°C, and the minimum concentration of Gal-3 (or mutants) required for agglutination was determined by serial dilution (Fig. 1*D*).

To assess intermolecular CRD–NT–CRD interactions, agglutination was performed with human erythrocytes type AB in the presence or absence of CRD or NT or combinations thereof as indicated. Agglutination was allowed to proceed for 60 min at 4°C, followed by photography (Fig. 4*G*) or confocal imaging (*SI Appendix*, Fig. S7*J*) using a confocal microscope (LSM 880, Zeiss).

Endocytosis assays. This assay was performed as previously described (1). HMEC-1 cells (4 x 10^5/well) were seeded in a 6-well plate and grown overnight. The medium was removed, and the cells were rinsed. To each well, 2 ml of PBS containing 0.2 μM wild-type or mutant Gal-3 was added and incubated at 37°C for 30 min. In some instances, 2 mM Lac was included. After incubation, the cells were washed three times with 50 mM ascorbic acid at 4°C and then detached with a cell scraper, followed by lysis for Western blotting. An aliquot (15 μl) of the medium from each incubation was also examined by Western blotting.

Turbidity assays. Turbidity was measured by absorption at 400 nm in 96-well plates using a Tecan Spark 10M microplate reader.

Dynamic light scattering (DLS) measurements. We performed DLS experiments using a NanoBrook omni (Brookhaven) instrument. Each measurement consisted of 3 runs. The analysis was operated at an angle of 90°, and the data were collected at 37°C.

Confocal imaging and fluorescence recovery after photo-bleaching (FRAP). Cells or droplets were observed on a glass slide for differential interference contrast (DIC) or fluorescence imaging using a Zeiss LSM 880 with a Plan-Apochromat 63x/1.40 oil objective at room temperature. The GFP fluorescence was imaged under 488 nm excitation and 541 nm emission. The autofluorescence of erythrocytes was imaged under 561 nm excitation and 640 nm emission. FRAP experiments were performed with the same microscope and lenses. Defined regions were photo-bleached at 488 nm. For bleaching, 45-80x repeats at laser powers of 10%–55% were used. The fluorescence intensities in these regions were collected every 2 s. For quantitative analysis, the fluorescence intensity before photo-bleaching was normalized to 1, and more than 5 cells or beads for each protein were assayed. The results are expressed as the mean ± SD. Image intensity was measured by the mean ROI and further analysed by GraphPad Prism 6.

Western blotting. Cells were lysed with RIPA buffer (50 mM Tris/acetate, pH 7.4, 0.5% Triton X-100, 150 mM sodium chloride, 0.1 mM PMSF, protease inhibitor cocktail and 2 mM Na_3VO_4), separated by 12% SDS/PAGE and transferred to PVDF membrane. The membranes were blocked and incubated with initial antibodies overnight at appropriate dilutions. After incubation with the secondary antibody for 1 h at room temperature, membranes were processed for scanning using the automatic chemiluminescence imaging analysis system (Tanon 5200, Shanghai, China).

Sample preparation for phase separation. All purified proteins were prepared in buffer containing 25 mM HEPES pH 7.5, 150 mM NaCl, and 1 mM DTT. Before each experiment, proteins were centrifuged at 10000 ×g at 4°C for 10 min to remove possible non-specific aggregates. Then, proteins were mixed or diluted to reach designated concentrations.

Phase separation induced by high salt. To investigate the effect of salt and protein concentrations on phase separation, full-length or truncated Gal-3 was diluted to the indicated concentrations, and the concentration of NaCl was adjusted to 1.0 M, 1.5 M, 2.0 M or 2.5 M NaCl with 4 M NaCl. After 5 min of incubation at 37°C, droplets were observed under a microscope.

For other measurements, proteins (full-length or truncated Gal-3, Gal-3(L203A), Gal-3(R186S), GFP−Gal-3 or proline mutants) diluted to 40 μM in 2.5 M NaCl were incubated

at 37°C for 5 min. Phase separation was assessed either by observing the images under a microscope (Thermo EVOS FL Auto microscope with 20x objective) or by measuring the turbidity at 400 nm or the sizes with DLS.

Phase separation induced by glycan in solution. Galectins (Gal-1, Gal-2, Gal-3, Gal-3 truncates or mutants) and glycoproteins (CD146, CD146 D1 to D4, PNGase F-treated CD146, CD45, CD71 or CD7) were all prepared in buffer containing 25 mM HEPES, pH 7.5, 150 mM NaCl and 1 mM DTT and diluted to reach the designated concentrations. Phase separation was induced by mixing a galectin with a glycoprotein and sometimes 4 mM Lac or Suc at 37°C for 5 min and assessed either by observing the confocal and DIC images under a microscope (LSM 880, Zeiss) or by measuring the turbidity at 400 nm or the sizes with DLS.

To investigate the effect of temperature on droplet stability (Fig. 2*C*), 20 μM Gal-3 and 100 nM CD146 were incubated at 37°C for 5 min followed by turbidity measurement. Then, the solution was placed in a 4°C incubator and measured again at 8 h and 24 h, respectively.

Assessment of cell surface Gal-3 oligomerization/condensation by FRAP. Jurkat cells were fixed with 4% paraformaldehyde at room temperature for 15 min, washed with PBS three times, placed in PBS, and stored at 4°C. Human erythrocytes type AB were fixed as described by Gao et al (5). Lac-coated beads were prepared with Lac and Sepharose CL-6B according to a previously published protocol (6). CD146-coated beads were prepared with CD146 and nickel beads. Nickel beads (100 μl) were incubated with 10 μg/ml CD146 at 4°C for 1 h, washed with PBS, placed in PBS, and stored at 4°C.

The fixed Jurkat cells and human erythrocytes type AB, Lac-coated beads or CD146-coated beads (20 μl each) were mixed with 20 μl of PBS buffer containing GFP−Gal-3, GFP−Gal-3(R186S), GFP−Gal-3(L203A), GFP−Gal-3Δ68 or GFP-CRD and incubated at 37°C for 5 min. All GFP-tagged proteins were diluted to a final concentration of 0.5 μM unless indicated otherwise. In some cases, 4 mM Lac was added. To assess the NT−CRD interaction (Fig. 3 *J* and *K*), fixed Jurkat cells were mixed with PBS buffer containing 2 μM CRD, 1 μM GFP-NT or their combination. After incubation, 20 μl of reaction was transferred to a coverslip and observed under a confocal microscope (LSM 880, Zeiss) followed by FRAP analysis.

Assessment of Gal-3 oligomerization/condensation on the endomembranes by FRAP. pcDNA 3.1 eukaryotic expression plasmids encoding GFP−Gal-3, GFP−Gal-3(L203A), GFP−Gal-3(R186S), and GFP−Gal-3Δ68 were synthesized by Synbio Technologies (Suzhou, China). HEK 293T cells (5 x 10^4/well) seeded on the slide in a 24-well plate were

transfected with plasmids using the Lipofectamine 3000 transfection reagent (Invitrogen) and Opti MEM (Gibco, NY, USA) according to the manufacturer's instructions. Twenty-four hours after transfection, cells were treated with 1 mM LLOMe for 2 h followed by confocal and DIC imaging under a microscope (LSM 880, Zeiss) and FRAP analysis.

Assessment of cell surface Gal-3 oligomerization/condensation by flow cytometry. Jurkat cells were fixed with paraformaldehyde as described above. Fixed cells (2×10^6) were incubated in 500 µl of PBS buffer containing 0.01 or 0.1 µM "hot" protein (GFP–Gal-1, GFP–Gal-3, GFP–Gal-3(R186S), GFP–Gal-3(L203A), GFP-CRD, GFP-NT or FITC–Gal-3) with or without 0.05, 0.1, 0.2, and 1.0 µM "cold" protein [non-fluorescent Gal-1, Gal-3, Gal-3(R186S), Gal-3(L203A), CRD or CRD(L203A)] at 4°C for 30 min in the dark. Inhibitor 4 mM Lac was added in some cases. After incubation, cells were harvested, washed once with PBS, and analysed with a BD Accuri™ C6 flow cytometer (excitation at 488 nm, emission at 535 nm) (Fig. 4 *A*-*F*). For each sample, 1×10^4 cells were analysed using BD Accuri™ C6 software.

Assessment of cell surface Gal-3 oligomerization/condensation by Western blotting. HMEC-1 cells (1×10^6/well) were seeded in a 6-well plate and grown overnight. The medium was removed, and the cells were rinsed. To each well, 2 ml of PBS containing "hot" proteins (0.4 µM His-Gal-3 or 10 µM His-NT) with or without "cold" proteins (Gal-3, His-CRD or His-NT at the concentrations indicated) was added and incubated at 4°C for 30 min. In some cases, 3 mM Lac was added. After incubation, the cells were washed twice with PBS at 4°C and then detached with a cell scraper, followed by lysis for Western blotting (*SI Appendix*, Fig. S7 *G*-*I*).

To compare the association of wild-type and mutant proteins with HMEC-1 cells (Fig. 5*H*), 2 ml of PBS containing 0.1 µM Gal-3 or mutants was added to each well, otherwise identical to the procedure described above. To compare the association of wild-type and mutant proteins with Jurkat cells (Fig. 5*H*), 2×10^6 cells were incubated in 500 µl of PBS containing 0.1 µM Gal-3 or mutants at 4°C for 30 min. Then, the cells were washed twice with PBS, followed by lysis for Western blotting. An aliquot (15 µl) of the medium from each incubation was also examined by Western blotting.

Glycan array studies. A 100 *N*-glycan-based glycan array from Kerixin Biological Technology Co., Ltd. (Nanjing, China) was used to assess whether mutation of specific NT prolines modifies the glycan binding profile. Glycan structures in the array are shown in *SI Appendix*, Fig. S13*A*. Measurements and data analysis were performed by Kerixin Biological Technology Co., Ltd. (Nanjing, China). In brief, wild-type Gal-3 and proline mutants were labelled with Cy3 and diluted to 25 µg/ml with incubation buffer (Kerixin

Biological Technology Co., Ltd). Each of the labelled proteins (200 µl) was added to a subarray and incubated for 1 h in the dark. After removing unbounded protein, the array was washed twice with TBST buffer (20 mM Tris-HCl, pH 7.6, 150 mM NaCl, 0.05% Tween), once with distilled water, and finally dried. The dried array was scanned using a microarray scanner (LuxScan 10K/A, CapitalBio Corporation, Beijing, China) and analysed using LuxScan 3.0 software.

Biolayer interferometry (BLI) assay. BLI assays were performed using a Fortebio Octet RED 96 instrument as described previously (4). To measure GP-triggered Gal-3 oligomerization/condensation on the solid surface, we coated (or loaded) sensors with CD146 and subsequently exposed the sensors to Gal-3 for association and then to buffer without Gal-3 for dissociation. Prior to measurements with CD146-coated sensors, non-coated sensors were tested for the absence of non-specific Gal-3 binding (*SI Appendix*, Fig. S8 *A* and *B*). Two types of sensors (both from Fortebio) were used. Ni-NTA sensors were used for Gal-3 mutants P17A, P19A, P23A, P30A, P42A, P46A, P50A, P51A, and P60A because these mutants did not show non-specific binding to Ni-NTA sensors. SA sensors were used for Gal-3 mutants P37A, P55A, P59A, P64A, and P67A because they did show non-specific binding to Ni-NTA sensors but not to SA sensors. Ni-NTA sensors were coated with 10 µg/ml His-tagged CD146 (in PBST) and SA sensors with 10 µg/ml biotin-labelled CD146 (in PBST). Gal-3 or Gal-3 mutants was diluted in PBST, and a set of concentrations (0, 500, 1000, 1500, 2000, 2500, 3000, and 3500 nM) for each species of Gal-3 was assessed. The program includes the following steps: loading CD146 for 150 s or 60 s, setting in PBST for 60 s, Gal-3 association for 120 s, and Gal-3 dissociation for 120 s. The sensors were regenerated as previously described.

The entire process was recorded as a sensorgram with the *x*-axis showing the time course and the *y*-axis showing response to change in sensor thickness that reflect the extent of Gal-3 binding to the sensor. To determine binding parameters (e.g., dissociation constants K_Ds), data were analysed using ForteBio Data Analysis Software 7.0.

Microscale thermophoresis (MST). MST was carried out using a Monolith NT.115 instrument (NanoTemper Technologies GmbH, München, Germany). His-tagged Gal-3 NT, CRD or CRD(L203A) was fluorescently labelled (referred to as *NT, *CRD or *CRD(L203A), respectively) with the MO-L018 His-Tag Labelling Kit (NanoTemper Technologies) according to the manufacturer's instructions and adjusted to 50 nM in PBST. The unlabelled ligands (peptides, NT, CRD, NT mutants) were diluted in PBST to generate a gradient of 16 concentrations. Equal volumes of *CRD, *CRD(L203A) or *NT and the unlabelled ligands were mixed and transferred into standard treated capillaries (MO-K022, NanoTemper Technologies). Measurements were performed at 25°C using a Monolith

NT.115 and MO. Control software (excitation power 100%, MST power 40%). Data were analysed using MO. Affinity Analysis software and Origin 8.0.

Isothermal Titration Calorimetry (ITC). ITC experiments were performed using a Nano ITC 601000 instrument (TA Instruments, USA). Wild-type Gal-3 and mutants (P17A, P19A, P23A, P30A, P37A, P42A, P46A, P50A, P51A, P55A, P59A, P60A, P64A, P67A, P64H, and L203A) were dialysed into PBS (pH 7.4) and adjusted to 0.2 mM. Glycans (Lac, LacNAc, and $(LacNAc)_3$) were dissolved in the same buffer at 2.4 mM. Titrations were performed at 37^{o}C by injecting 50 µl aliquots of the glycan into the protein solution at time intervals of 300 s with a stirring speed of 300 rpm. In addition, relevant reference control experiments, in which the glycan was titrated into PBS, were also conducted. For each ITC dataset, the reference data was subtracted from the raw data to obtain the net result for the final fitting analysis. The net result was analysed using TA Instruments Nano Analyze^{TM} software.

Sedimentation assay. To investigate stoichiometry, Gal-3 and CD146 were mixed in different proportions as indicated and incubated at 37°C for 5 min to allow phase separation. The samples were centrifuged at 10000 ×g for 5 min. After centrifugation, the supernatant and pellet were immediately separated. The pellet fraction was washed once and thoroughly resuspended in buffer containing 25 mM HEPES pH 7.5, 150 mM NaCl, and 1 mM DTT so that the volume was the same as the supernatant fraction. The amounts of Gal-3 and CD146 in the supernatant and pellets were detected by Western blotting.

NMR spectroscopy. Wild-type (WT) human Gal-3 or human Gal-3 NT proline mutants were dissolved at a concentration of 20 µM in 20 mM potassium phosphate buffer at pH 6.9, made up using a 95% H_2O/ 5% D_2O mixture. Natural abundance ^{1}H-^{15}N HSQC NMR experiments were performed on WT Gal-3 and Gal-3 NT proline mutants, and the results were compared. ^{1}H and ^{15}N resonance assignments for recombinant human Gal-3 were previously reported (7). NMR assignments of Gal-3 NT proline mutants were made by comparison to those for WT Gal-3. The assignment of CRD resonances in Gal-3 NT mutants was relatively straightforward and complete, whereas those of a number of NT residues in the mutants could not be made for various reasons and thus are incomplete in many instances.

NMR experiments were carried out at 30°C on a Bruker 850 MHz NMR spectrometer equipped with an H/C/N triple-resonance probe and *x*/*y*/*z* triple-axis pulse field gradient unit. A gradient sensitivity-enhanced version of the two-dimensional ^{1}H-^{15}N HSQC experiment (32 scans per transient) was applied with 256 (*t*1) x 2048 (*t*2) complex data points in ^{15}N and ^{1}H dimensions, respectively, and a sweep width of 16 ppm in the ^{1}H

dimension and 30 ppm in the ^{15}N dimension. Raw data were converted and processed by using NMRPipe (8) and were analysed by using NMRview (9).

Statistical analyses. All data are presented as the mean ± SD/SEM. GraphPad Prism 6 software was used for statistical analysis. At least three independent samples were included for statistical analysis between two different groups. Statistical analysis was performed with Student's two-tailed *t*-test. *, **, ***, and **** denote $p < 0.05$, $p < 0.01$, $p < 0.001$, and $p < 0.0001$, respectively.

Supplementary Figures

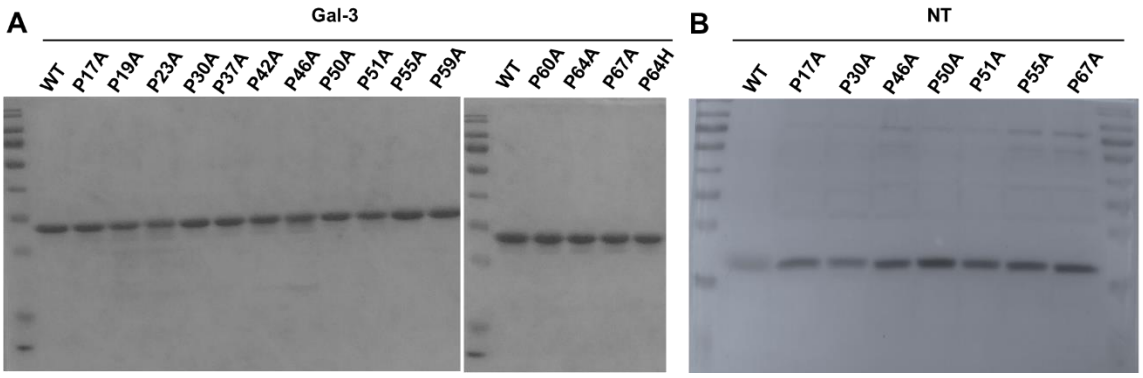

Fig. S1. Detection of protein purity. Related to Fig. 1, 5, and Table 1. Wild-type (WT) and proline mutants of the full-length Gal-3 (*A*) and NT fragment (*B*) were assessed by SDS-PAGE with Coomassie blue staining.

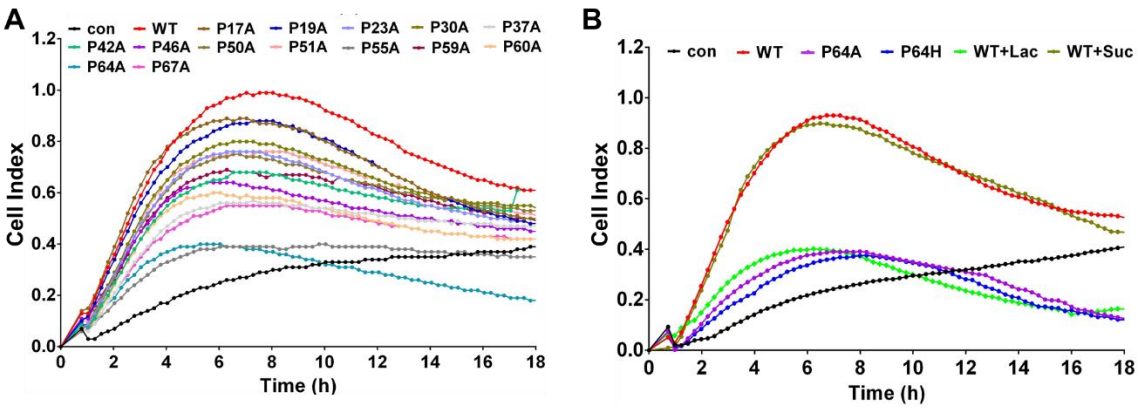

Fig. S2. Effect of proline mutation on Gal-3-induced HMEC-1 migration. Related to Fig. 1*A*. HMEC-1 migration induced by 0.7 μM wild-type (WT) Gal-3 (with or without Lac or Suc) or Gal-3 NT proline mutants was monitored in real time by using xCELLigence RTCA DP (*A* and *B*). Quantitative data are shown in Fig. 1*A*. Con, without attractant.

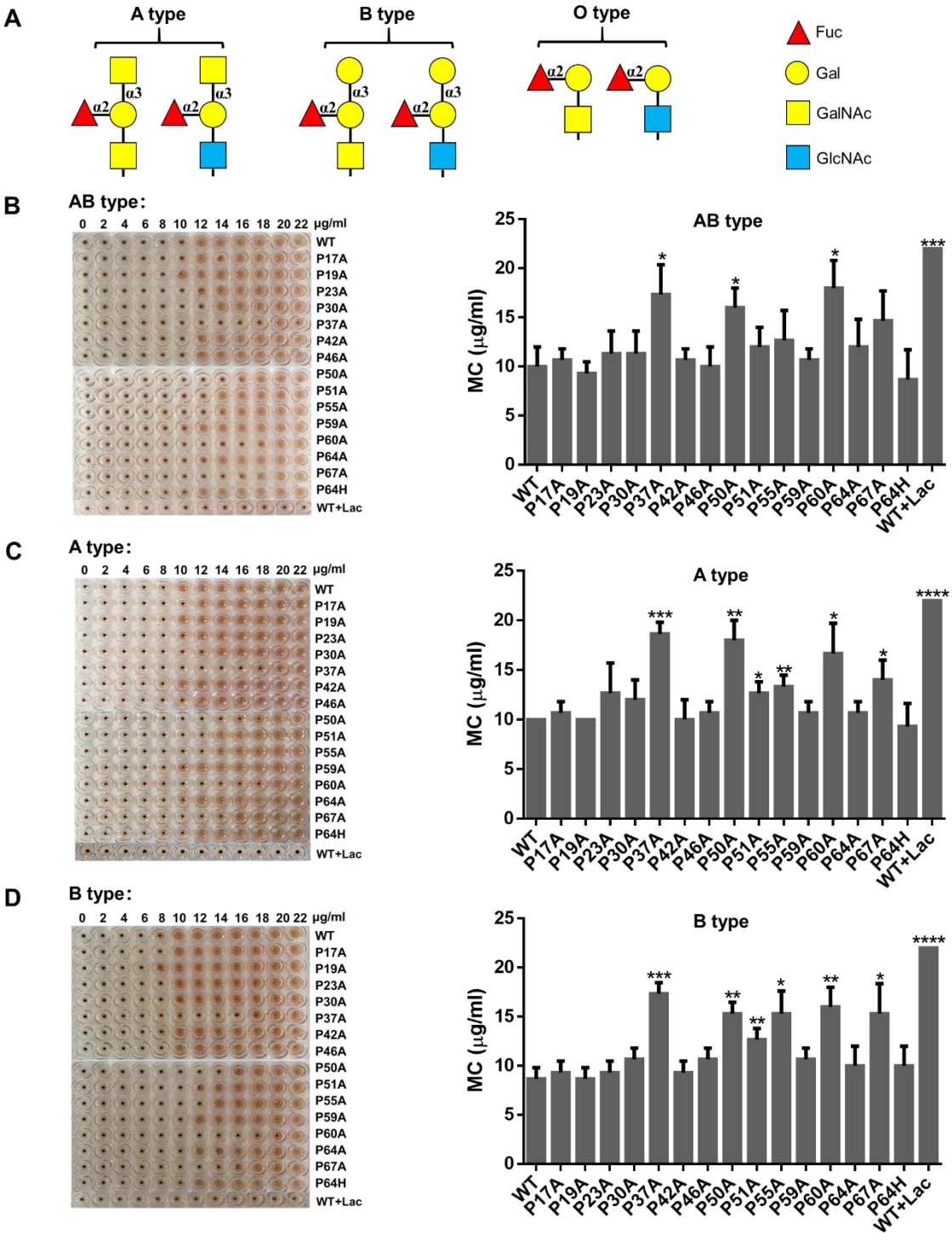
A
A type
B type
O type
α2
α3
Fuc
Gal
GalNAc
GlcNAc
B
AB type:
0 2 4 6 8 10 12 14 16 18 20 22 μg/ml
WT
P17A
P19A
P23A
P30A
P37A
P42A
P46A
P50A
P51A
P55A
P59A
P60A
P64A
P67A
P64H
WT+Lac
AB type
MC (μg/ml)
C
A type:
A type
D
B type:
B type

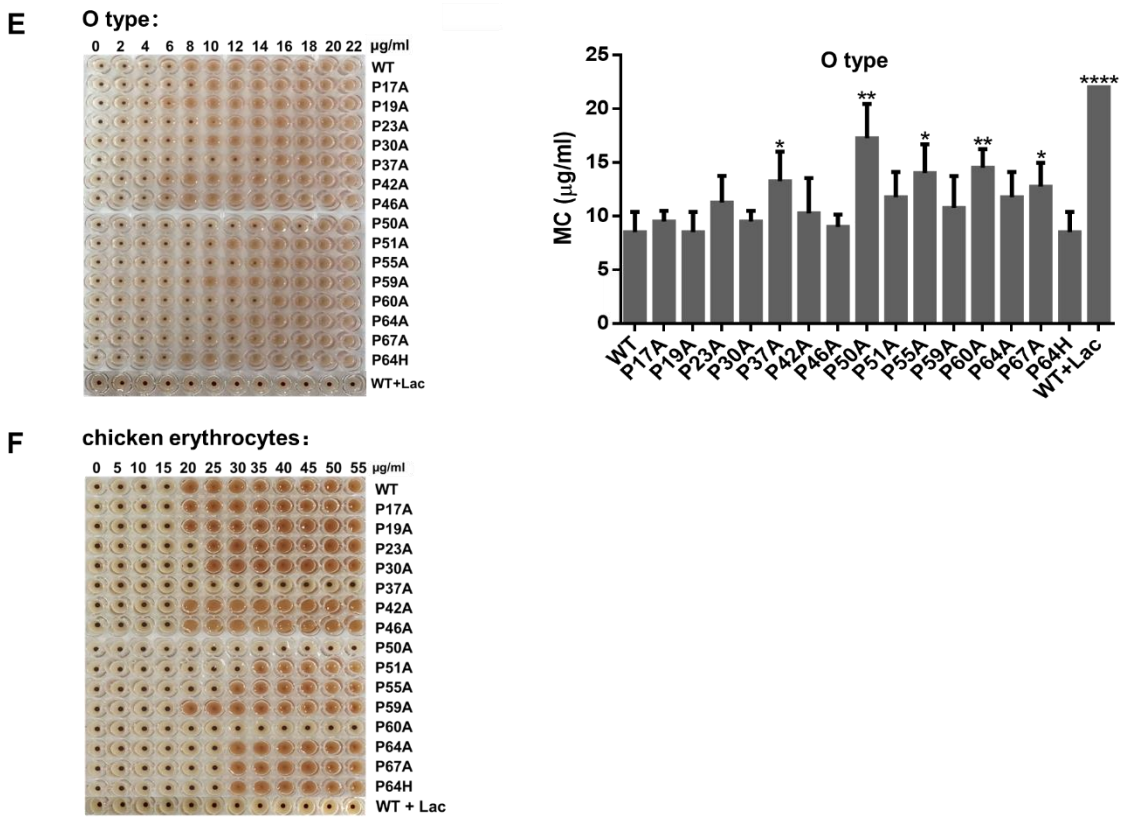

Fig. S3. Effect of proline mutation on Gal-3-induced hemagglutination. Related to Fig. 1*D*. (*A*) The structures of human A, B, O blood groups. (*B*-*F*) The agglutination of human erythrocytes type AB (*B*), type A (*C*), type B (*D*), type O (*E*), and chicken erythrocyte (*F*) was performed in the presence of increasing concentrations of wild-type (with or without 4 mM Lac) or mutant Gal-3. Quantitative data are shown as the mean ± SD (n=3). The quantitative data of *F* are shown in Fig. 1*D*. A comparison was made between the wild-type (WT) and each mutant. The *p* values were determined by Student's two-tailed *t*-test; *$p < 0.05$, **$p < 0.01$, and ***$p < 0.001$.

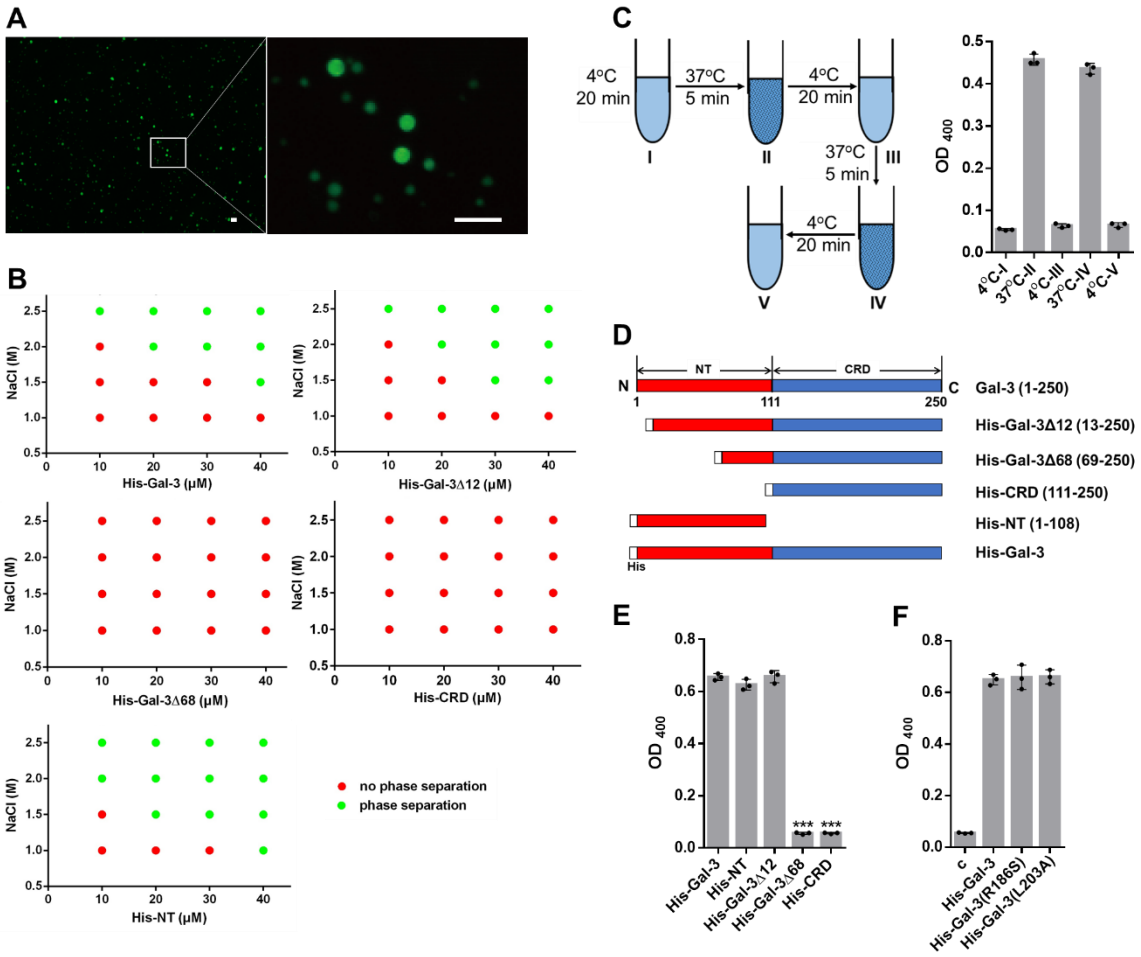

Fig. S4. Gal-3 LLPS induced by high salt. Unless otherwise indicated, all LLPS assays were performed with 40 μM Gal-3 or truncates in 2.5 M NaCl. (*A*) Microscopy images of the droplets formed by Gal-3 (0.5 μM GFP–Gal-3 + 40 μM Gal-3). Scale bar: 10 μm. (*B*) LLPS under different concentrations of Gal-3 variant and NaCl. (*C*) Effect of temperature on LLPS. (*D*) Schematic diagram of full-length and truncated Gal-3. (*E*) Turbidity of Gal-3 and truncates. (*F*) Turbidity of Gal-3 and mutants. Turbidity data are shown as the mean ± SD (n = 3). A comparison was made between the full-length Gal-3 and each truncate (or mutant). The *p* values were determined by Student's two-tailed *t*-test; ***$p < 0.001$.

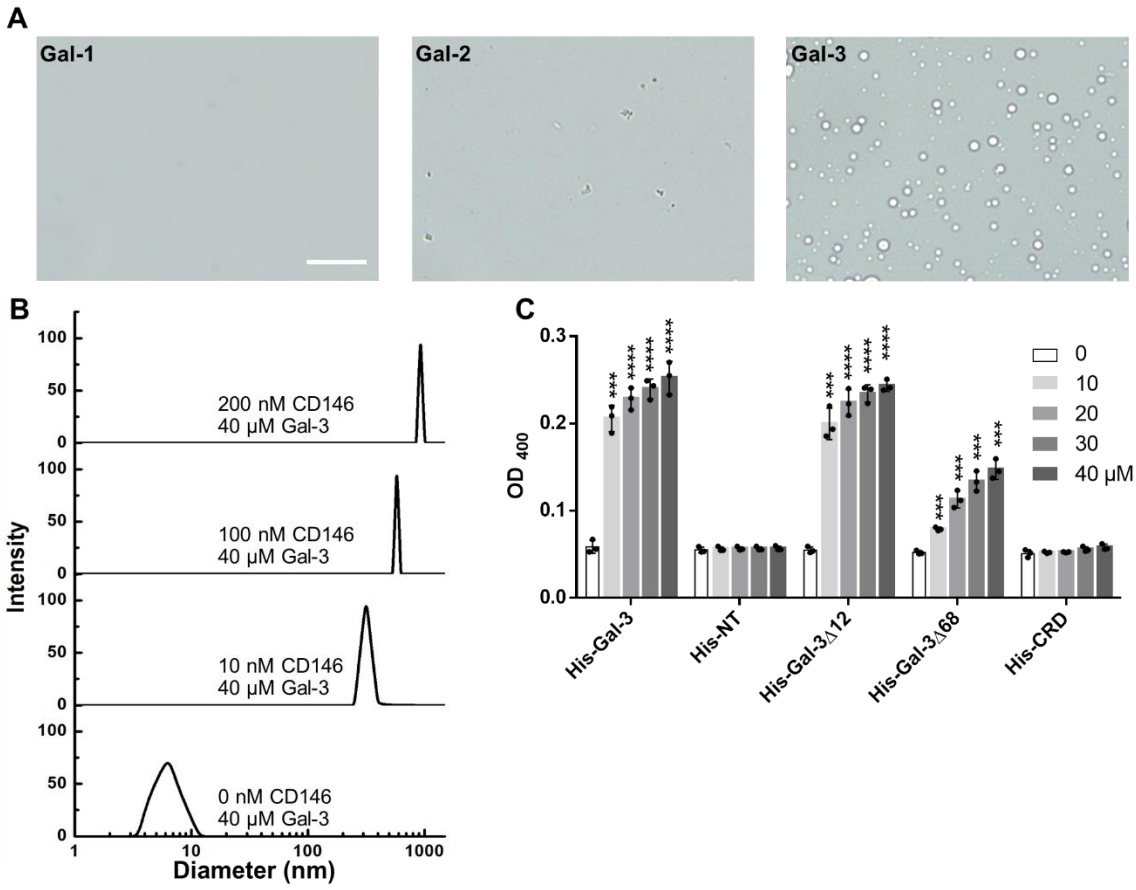

Fig. S5. LLPS induced by glycoproteins. Related to Fig. 2. (*A*) DIC images of 40 μM Gal-1, Gal-2 or Gal-3 in the presence of 200 nM CD146. Scale bar: 10 μm. (*B*) DLS of Gal-3 (40 μM) droplets in the presence of different concentrations of CD146. (*C*) Turbidity of full-length or truncated Gal-3 in the presence of 200 nM CD146. Data are shown as the mean ± SD (n = 3). The *p* values were determined by Student's two-tailed *t*-test; ***$p < 0.001$ and ****$p < 0.0001$.

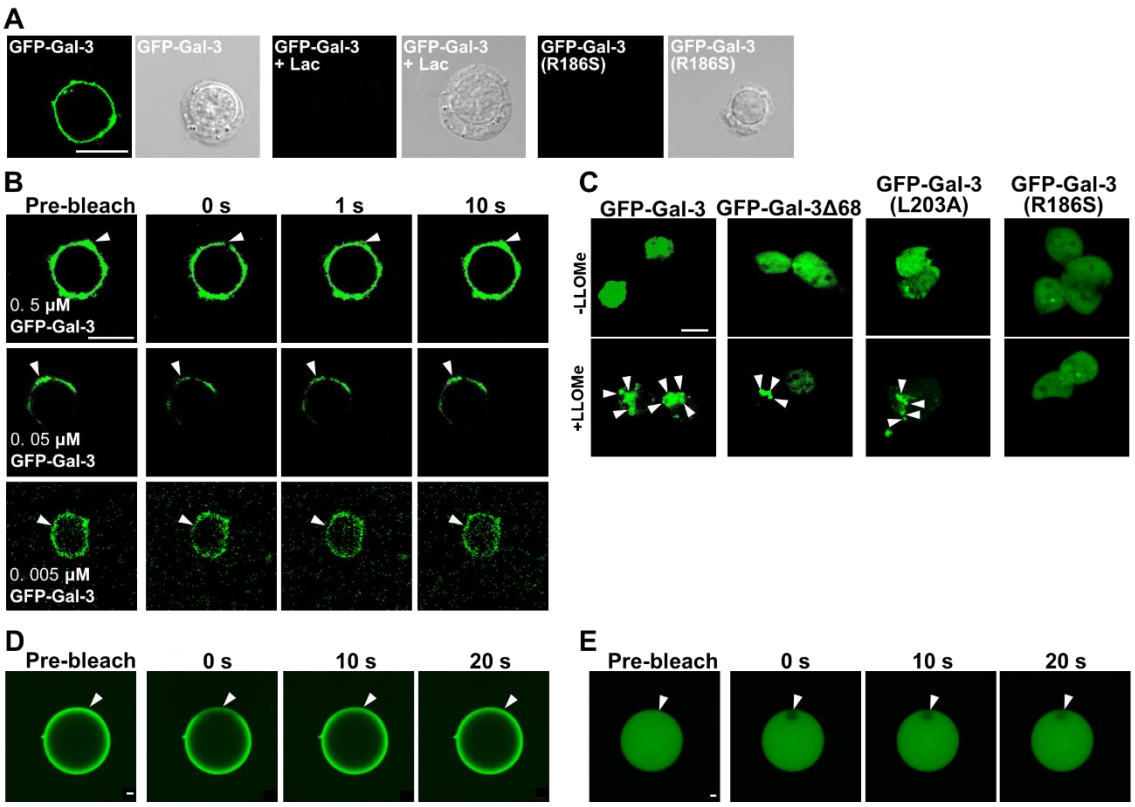

Fig. S6. Glycoprotein-triggered Gal-3 oligomerization/condensation on cell membranes. Related to Fig. 3. (*A*) Confocal and DIC microscopy of Jurkat cells incubated with GFP−Gal-3 or GFP−Gal-3(R186S) with and without Lac. (*B*) Confocal images before and after photo-bleaching of Jurkat cells with GFP−Gal-3. Quantitative FRAP data of *B* are shown in Fig. 3*B*. (*C*) Confocal and DIC of HEK 293T cells transfected with pcDNA 3.1-GFP−Gal-3, GFP−Gal-3Δ68, GFP−Gal-3(L203A) or GFP−Gal-3(R186S) and treated with or without LLOMe. GFP−Gal-3 (GFP−Gal-3Δ68 or GFP−Gal-3(L203A)) was accumulated in puncta upon LLOMe treatment (arrowheads). (*D*) Confocal images before and after photo-bleaching of CD146-coated beads with GFP−Gal-3. Quantitative FRAP data of *D* are shown in Fig. 3*G*. (*E*) Confocal images before and after photo-bleaching of Lac-coated beads with GFP−Gal-3. Quantitative FRAP data of *E* are shown in Fig. 3*H*. Scale bar: 10 μm.

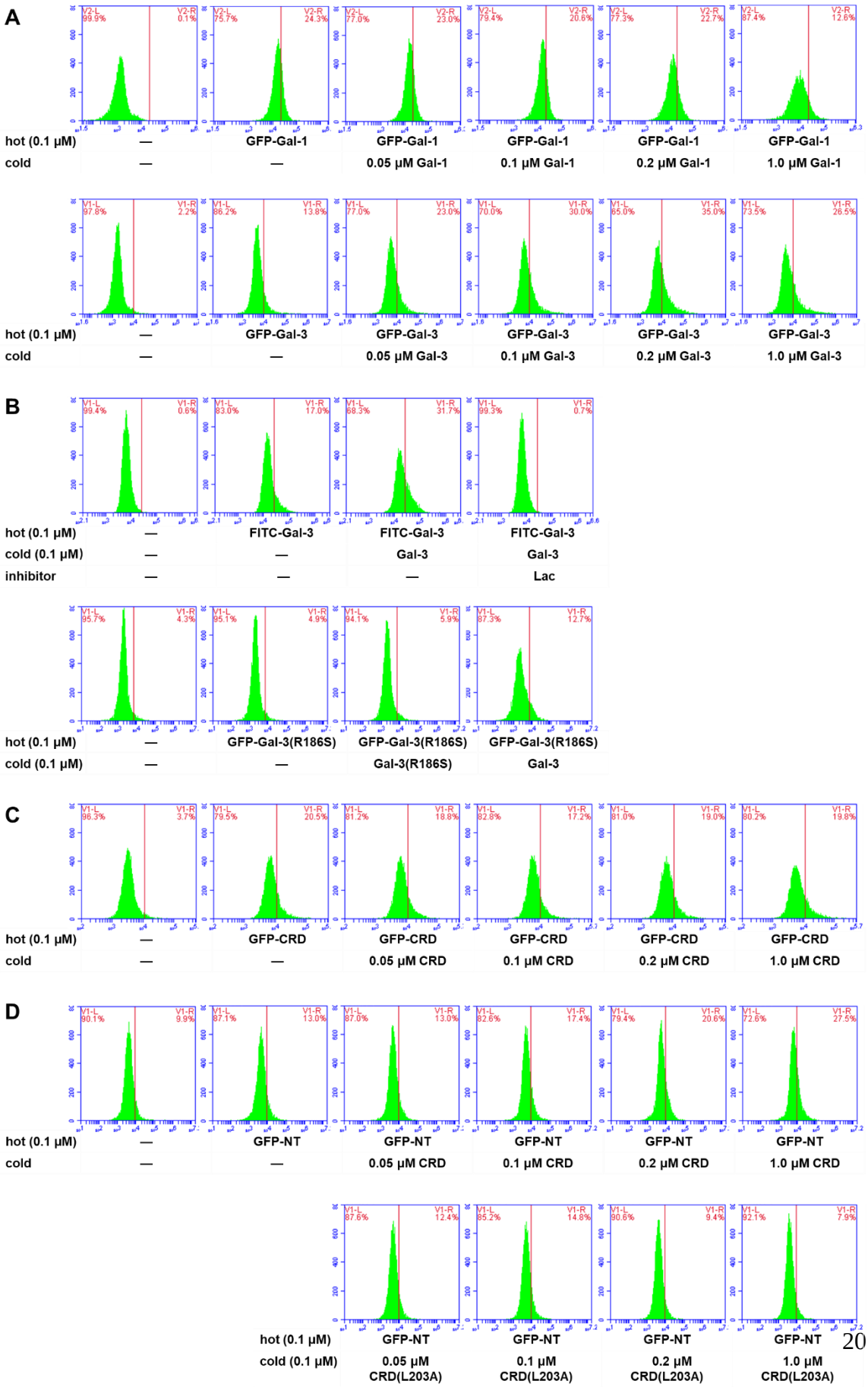
A
hot (0.1 μM) — GFP-Gal-1 GFP-Gal-1 GFP-Gal-1 GFP-Gal-1 GFP-Gal-1
cold — — 0.05 μM Gal-1 0.1 μM Gal-1 0.2 μM Gal-1 1.0 μM Gal-1
hot (0.1 μM) — GFP-Gal-3 GFP-Gal-3 GFP-Gal-3 GFP-Gal-3 GFP-Gal-3
cold — — 0.05 μM Gal-3 0.1 μM Gal-3 0.2 μM Gal-3 1.0 μM Gal-3
B
hot (0.1 μM) — FITC-Gal-3 FITC-Gal-3 FITC-Gal-3
cold (0.1 μM) — — Gal-3 Gal-3
inhibitor — — — Lac
hot (0.1 μM) — GFP-Gal-3(R186S) GFP-Gal-3(R186S) GFP-Gal-3(R186S)
cold (0.1 μM) — — Gal-3(R186S) Gal-3
C
hot (0.1 μM) — GFP-CRD GFP-CRD GFP-CRD GFP-CRD GFP-CRD
cold — — 0.05 μM CRD 0.1 μM CRD 0.2 μM CRD 1.0 μM CRD
D
hot (0.1 μM) — GFP-NT GFP-NT GFP-NT GFP-NT GFP-NT
cold — — 0.05 μM CRD 0.1 μM CRD 0.2 μM CRD 1.0 μM CRD
hot (0.1 μM) GFP-NT GFP-NT GFP-NT GFP-NT
cold (0.1 μM) 0.05 μM CRD(L203A) 0.1 μM CRD(L203A) 0.2 μM CRD(L203A) 1.0 μM CRD(L203A)

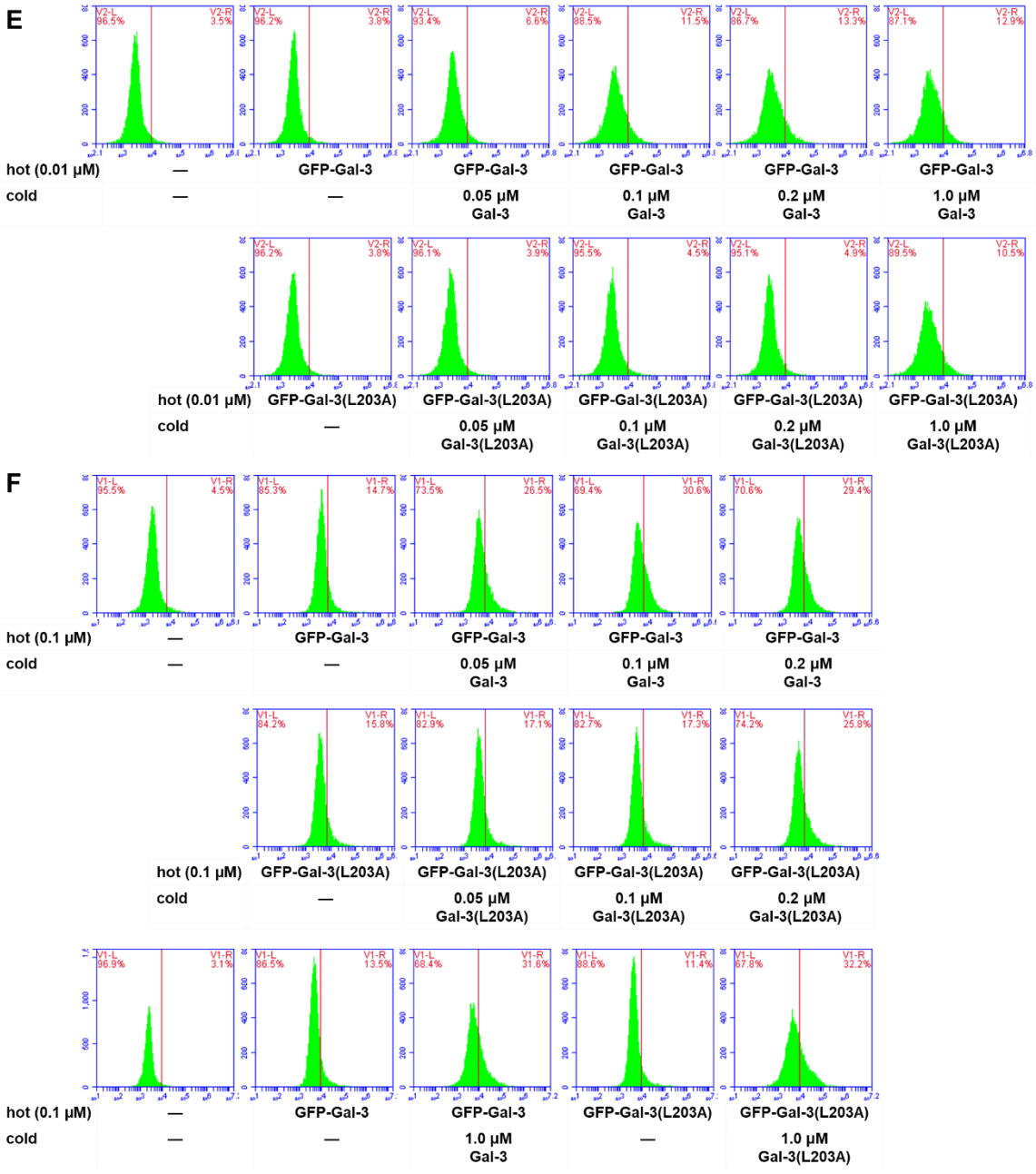
E
V2-L 96.5% V2-R 3.5%
V2-L 96.2% V2-R 3.8%
V2-L 93.4% V2-R 6.6%
V2-L 88.5% V2-R 11.5%
V2-L 86.7% V2-R 13.3%
V2-L 87.1% V2-R 12.9%
hot (0.01 μM) — GFP-Gal-3 GFP-Gal-3 GFP-Gal-3 GFP-Gal-3 GFP-Gal-3
cold — — 0.05 μM Gal-3 0.1 μM Gal-3 0.2 μM Gal-3 1.0 μM Gal-3
V2-L 96.2% V2-R 3.8%
V2-L 96.1% V2-R 3.9%
V2-L 95.5% V2-R 4.5%
V2-L 95.1% V2-R 4.9%
V2-L 89.5% V2-R 10.5%
hot (0.01 μM) GFP-Gal-3(L203A) GFP-Gal-3(L203A) GFP-Gal-3(L203A) GFP-Gal-3(L203A) GFP-Gal-3(L203A)
cold — 0.05 μM Gal-3(L203A) 0.1 μM Gal-3(L203A) 0.2 μM Gal-3(L203A) 1.0 μM Gal-3(L203A)
F
V1-L 95.5% V1-R 4.5%
V1-L 85.3% V1-R 14.7%
V1-L 73.5% V1-R 26.5%
V1-L 69.4% V1-R 30.6%
V1-L 70.6% V1-R 29.4%
hot (0.1 μM) — GFP-Gal-3 GFP-Gal-3 GFP-Gal-3 GFP-Gal-3
cold — — 0.05 μM Gal-3 0.1 μM Gal-3 0.2 μM Gal-3
V1-L 84.2% V1-R 15.8%
V1-L 82.9% V1-R 17.1%
V1-L 82.7% V1-R 17.3%
V1-L 74.2% V1-R 25.8%
hot (0.1 μM) GFP-Gal-3(L203A) GFP-Gal-3(L203A) GFP-Gal-3(L203A) GFP-Gal-3(L203A)
cold — 0.05 μM Gal-3(L203A) 0.1 μM Gal-3(L203A) 0.2 μM Gal-3(L203A)
V1-L 96.9% V1-R 3.1%
V1-L 86.5% V1-R 13.5%
V1-L 68.4% V1-R 31.6%
V1-L 88.6% V1-R 11.4%
V1-L 67.8% V1-R 32.2%
hot (0.1 μM) — GFP-Gal-3 GFP-Gal-3 GFP-Gal-3(L203A) GFP-Gal-3(L203A)
cold — — 1.0 μM Gal-3 — 1.0 μM Gal-3(L203A)

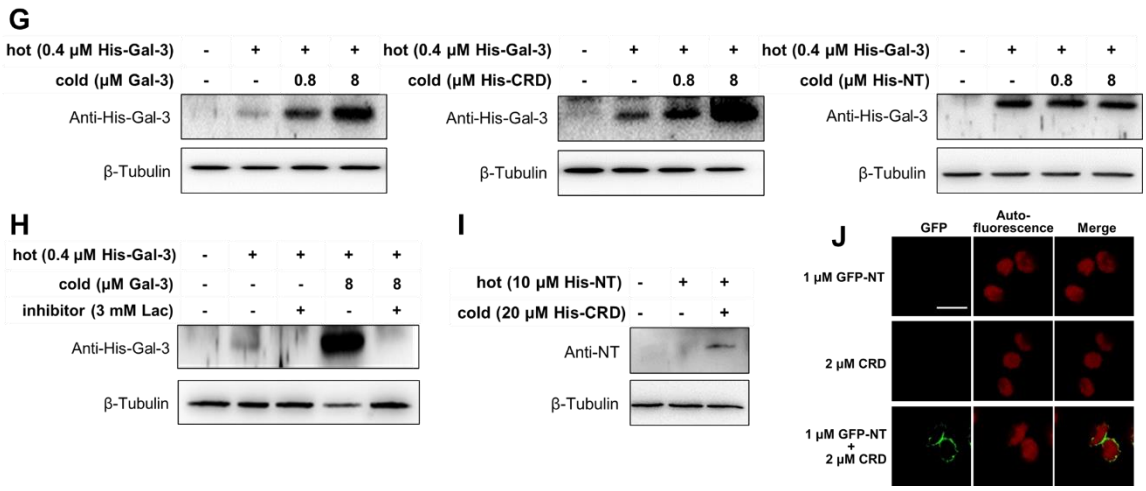

Fig. S7. Gal-3 oligomerization/condensation on the cell surface. Related to Fig. 4. (*A-F*) Fixed Jurkat cells were incubated with hot (fluorescently labelled) Gal-1 and Gal-3 variants with and without cold (non-fluorescently labelled) Gal-1, Gal-3 variants and inhibitor as indicated. The binding of the hot was analysed by flow cytometry. Quantitative data are shown in Fig. 4. Representative images shown in panels *A-F* correspond to Fig. 4 *A-F*, respectively. (*G-I*) HMEC-1 cells were incubated with hot Gal-3 (His-tagged Gal-3 variants) with and without cold Gal-3 variants and inhibitor as indicated. Binding of hot Gal-3 and its variants was detected by Western blotting. (*J*) The agglutination of human erythrocytes type AB was performed in the presence of CRD, NT or their combination. Confocal images showing fluorescent NT bridging the cells. Scale bar: 10 μm.

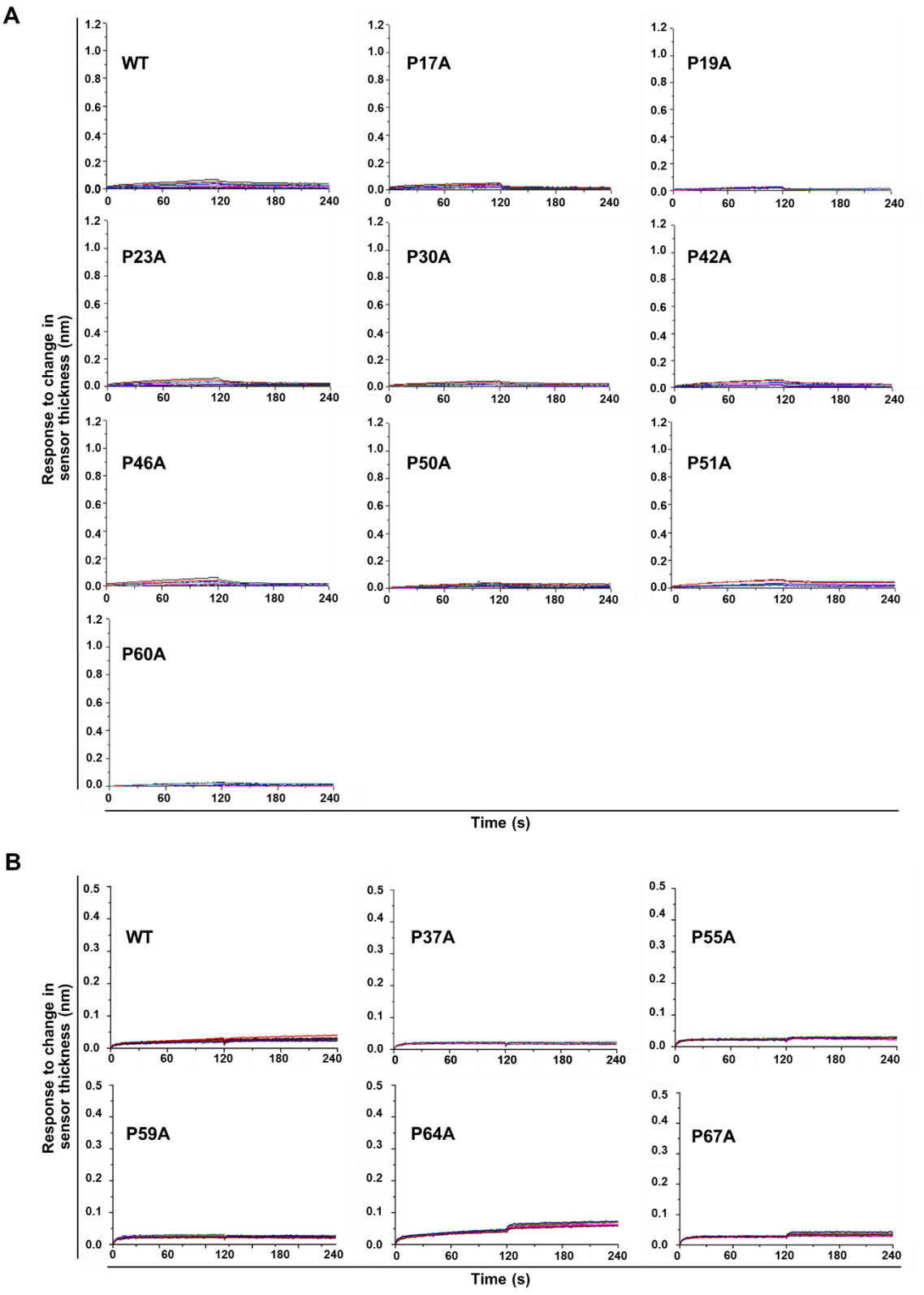
A
WT
P17A
P19A
P23A
P30A
P42A
P46A
P50A
P51A
P60A
Response to change in sensor thickness (nm)
Time (s)
B
WT
P37A
P55A
P59A
P64A
P67A
Response to change in sensor thickness (nm)
Time (s)

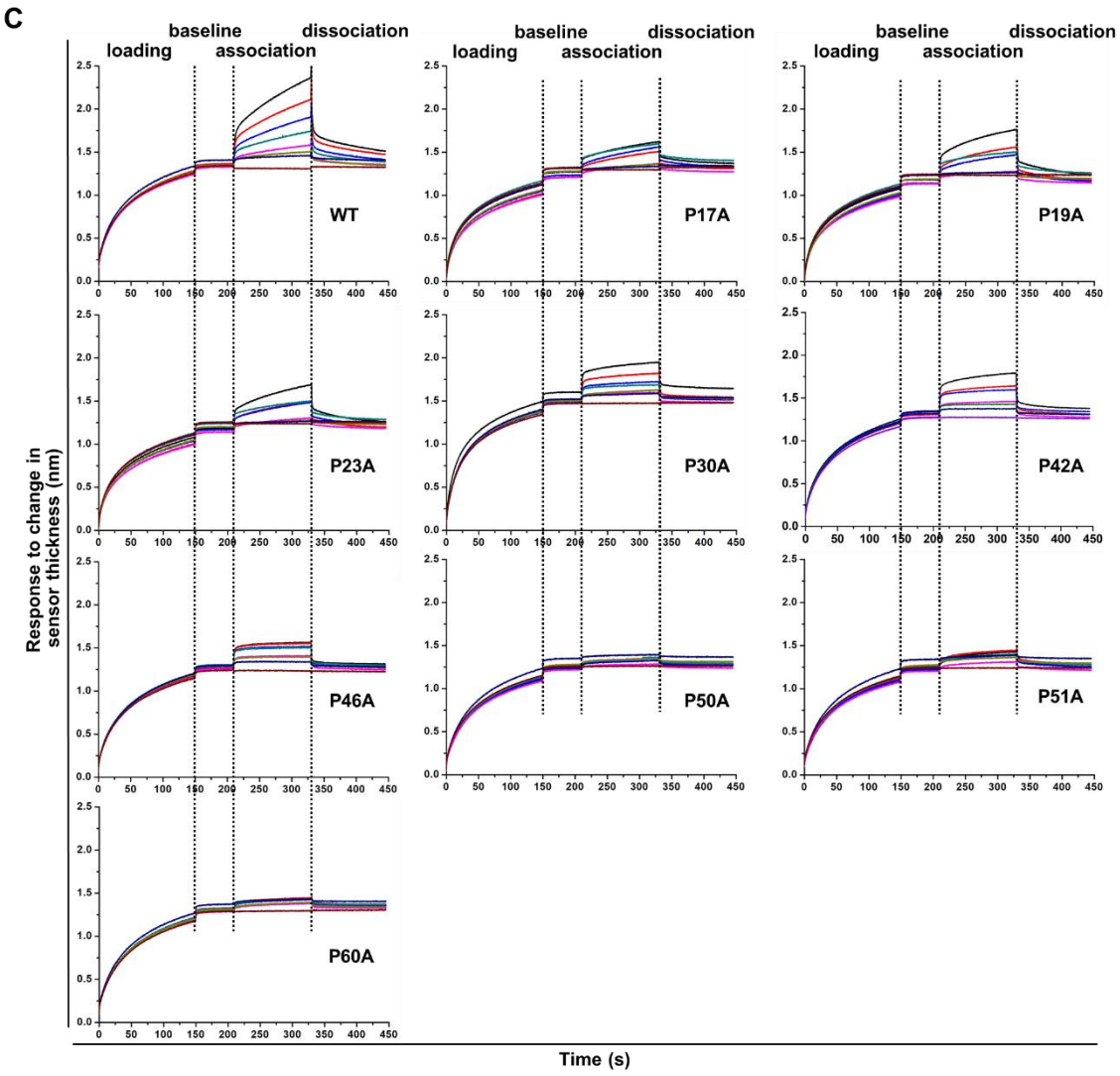
C
baseline
loading
association
dissociation
WT
P17A
P19A
P23A
P30A
P42A
P46A
P50A
P51A
P60A
Response to change in sensor thickness (nm)
Time (s)

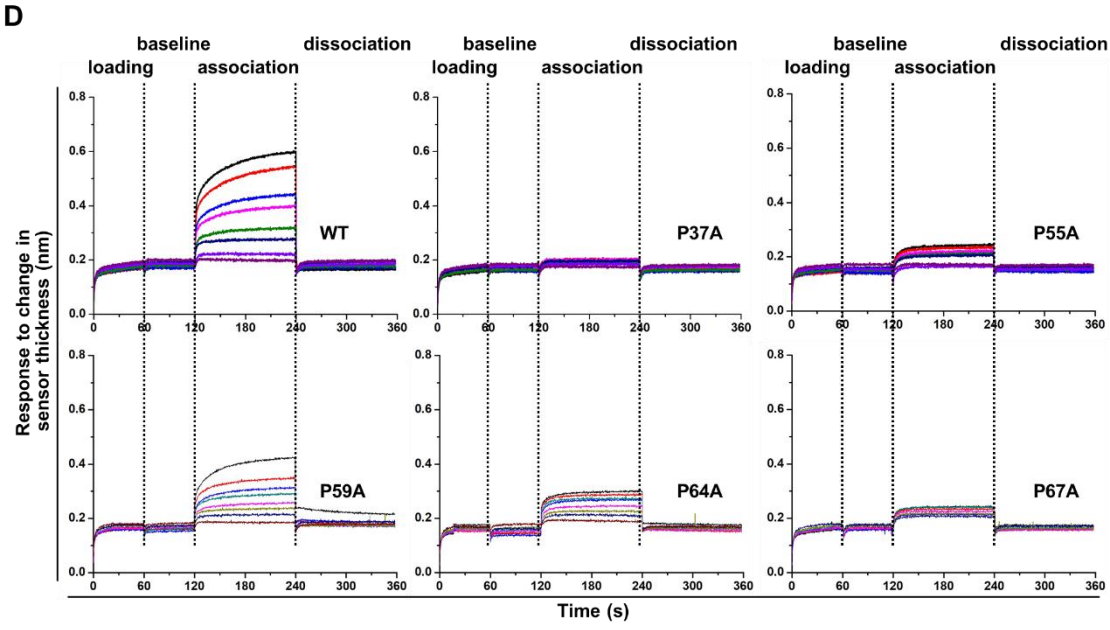
D
baseline
loading
association
dissociation
WT
P37A
P55A
P59A
P64A
P67A
Response to change in sensor thickness (nm)
Time (s)

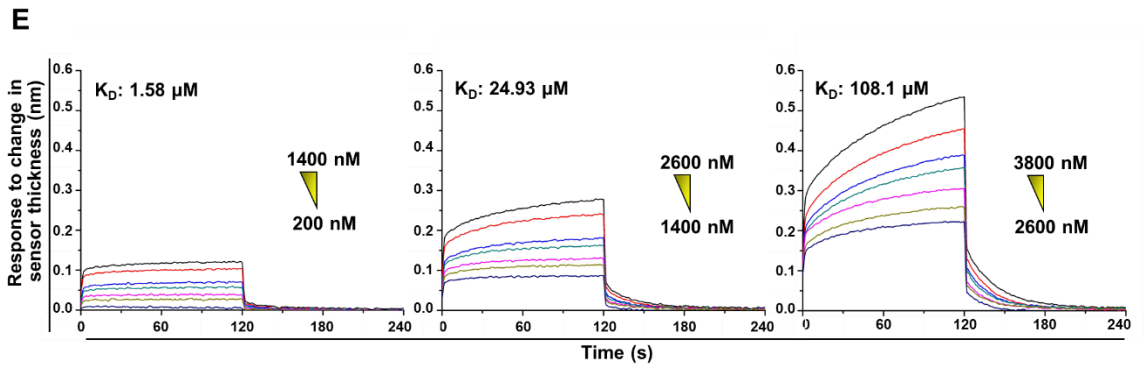

Fig. S8. Gal-3 condensation on CD146-coated biosensors assessed by BLI. Related to Fig. 5 *F* and *G*. (*A* and *B*) Assessment of non-specific binding with Ni-NTA (*A*) and SA sensors (*B*). Sensors (without CD146 coating) were directly placed in PBST buffer containing WT Gal-3 or mutants for 120 s and then transferred into PBST buffer without proteins for another 120 s. (*C* and *D*) Gal-3 condensation on CD146-coated biosensors. Full sensorgrams for Fig. 5 *F* and *G*. His-tagged CD146 or biotin-labelled CD146 was coated onto the Ni-NTA (*C*) or SA (*D*) sensors, respectively. WT Gal-3 and its mutants were tested at 0, 500, 1000, 1500, 2000, 2500, 3000, and 3500 nM as described in the Materials and Methods. (*E*) His-tagged CD146 was coated onto the Ni-NTA sensors and allowed to interact with Gal-3 within the ranges of 200-1400 nM, 1400-2600 nM, and 2600-3800 nM. K_D values are presented in each sensorgram.

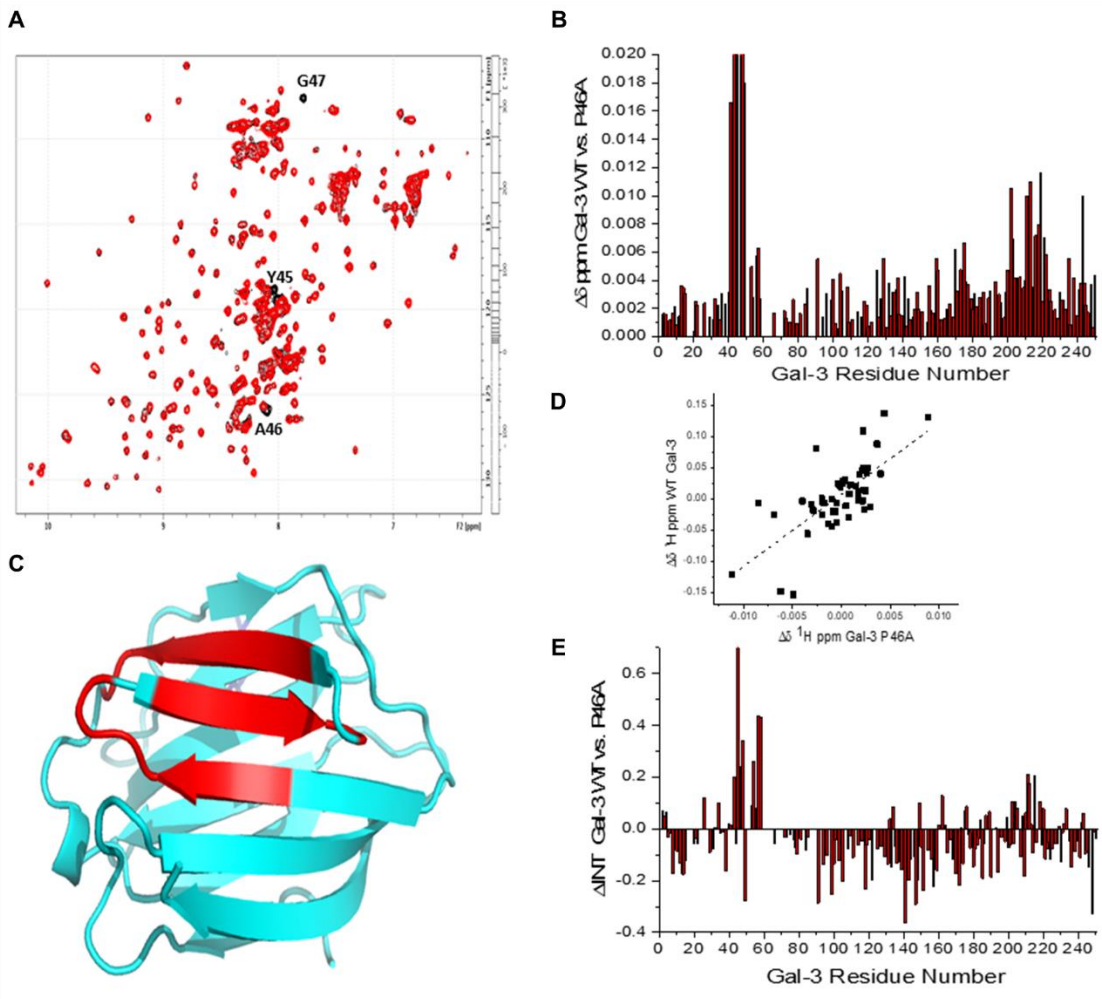
A
G47
Y45
A46
B
Δδ ppm Gal-3 WT vs. P46A
Gal-3 Residue Number
C
D
Δδ ¹H ppm WT Gal-3
Δδ ¹H ppm Gal-3 P46A
E
ΔINT Gal-3 WT vs. P46A
Gal-3 Residue Number

F

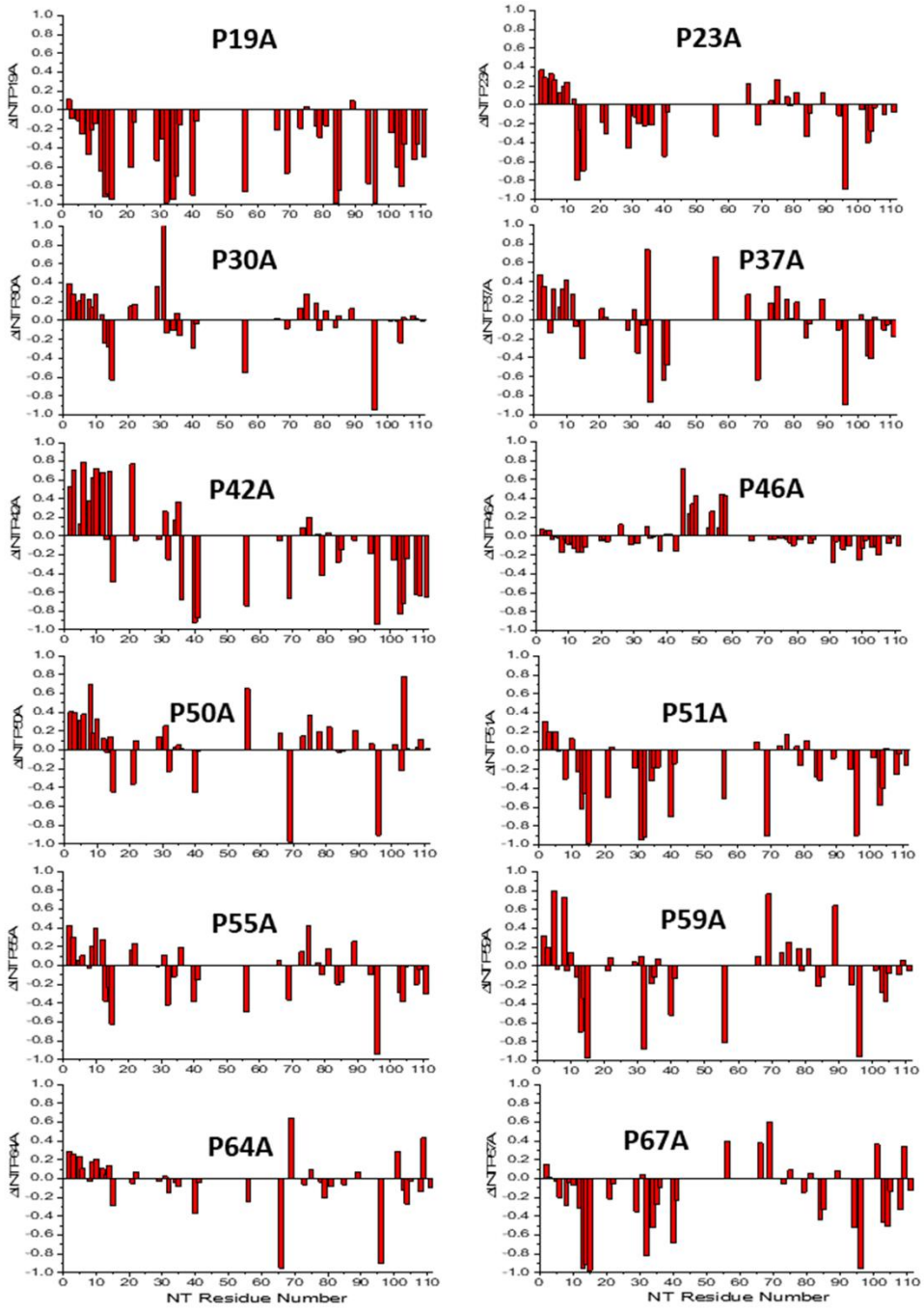
P19A
P23A
P30A
P37A
P42A
P46A
P50A
P51A
P55A
P59A
P64A
P67A
ΔNTP19A
ΔNTP23A
ΔNTP30A
ΔNTP37A
ΔNTP42A
ΔNTP46A
ΔNTP50A
ΔNTP51A
ΔNTP55A
ΔNTP59A
ΔNTP64A
ΔNTP67A
NT Residue Number
NT Residue Number

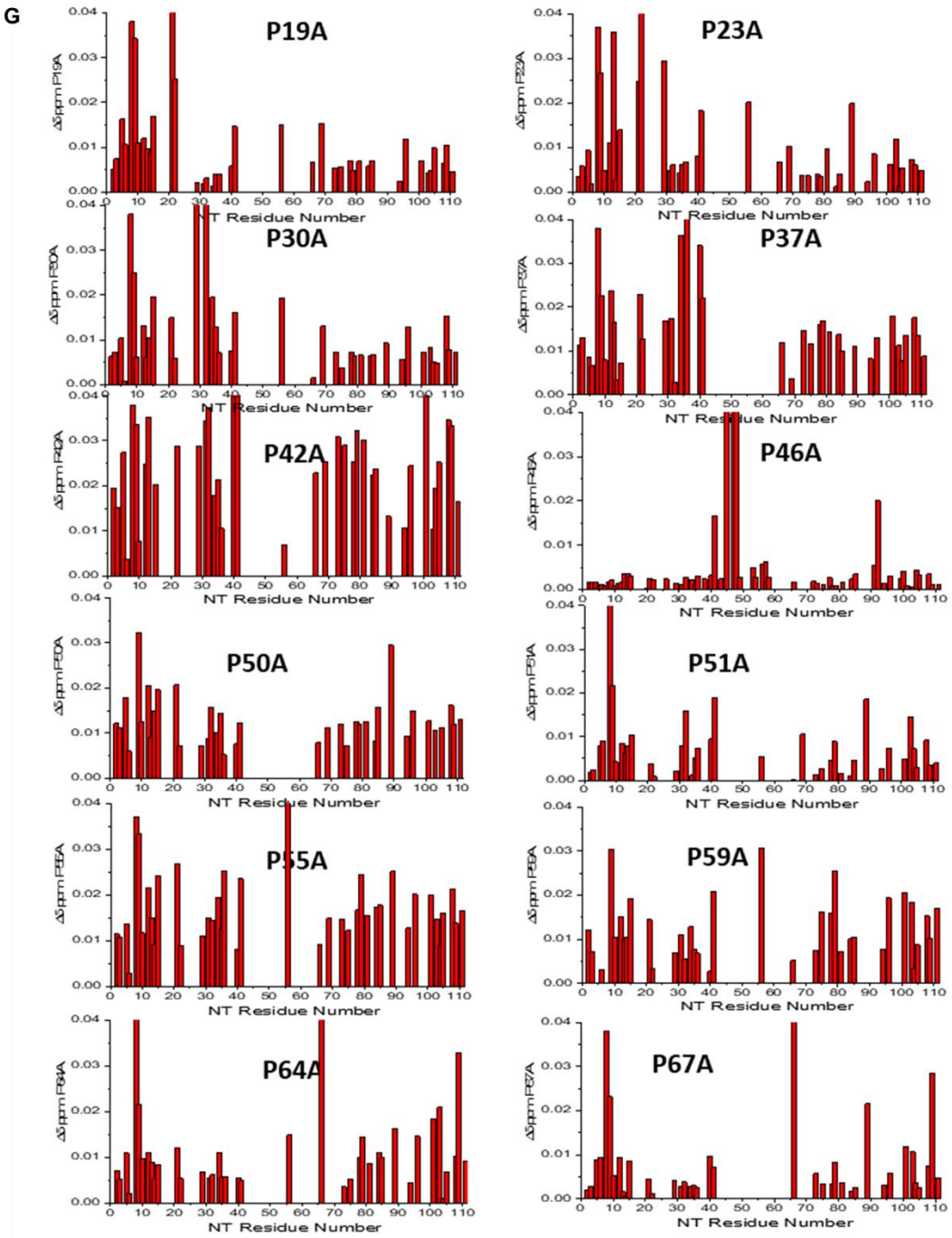

Fig. S9. Gal-3 NT prolines mediate NT–CRD exchange dynamics. (*A*) [^{1}H-^{15}N] HSQC spectra are shown for Gal-3 NT mutant P46A (20 μM, peaks in black) overlaid with that for WT Gal-3 (20 μM, peaks in red). The solution conditions were 20 mM potassium phosphate, pH 6.9. HSQC spectra (32 scans per transient) were acquired at 850 MHz (proton frequency) at 30°C with a sweep width of 16 ppm in the ^{1}H dimension (2,000 points) and 30 ppm in the ^{15}N dimension (256 points). (*B*) Chemical shift changes (Δδ) from these

HSQC spectra are plotted vs. the amino acid sequence of Gal-3 for the difference between WT Gal-3 and Gal-3 NT mutant P46A. (*C*) Using Δδ values, Gal-3 residues involved in binding CD146 are highlighted on the structure of the Gal-3 CRD (PDB code 1A3K (10)) in red (> 2SD above the average Δδ value) and cyan (Δδ values < the average). The structural orientation shows the F-face of the CRD β-sandwich, with the CRD S-face at the back. (*D*) A correlation plot is shown. Δδ values for F-face residues of WT Gal-3 relative to truncated CRD (*y*-axis) are plotted vs. Δδ values for F-face residues of Gal-3 NT mutant P46A relative to truncated CRD (*x*-axis). (*E*) ΔIntensity (ΔINT) values are plotted vs. the amino acid sequence of Gal-3. ΔINT was calculated as a fractional change by dividing the intensity of a given HSQC peak (WT Gal-3) by the intensity of the same peak in Gal-3 NT mutant P46A at the same protein concentration (20 μM) and subtracting the resulting value from one. Therefore, a value of one indicates that a resonance is no longer observed (i.e., highly broadened), a value of zero indicates no change in resonance intensity, and a negative value indicates that the resonance is increased in intensity (i.e., reduced broadening). (*F*) Resonance broadening or intensity changes (ΔINT) for residues within the Gal-3 NT. (*G*) Chemical shift changes (Δδ) for residues within the Gal-3 NT.

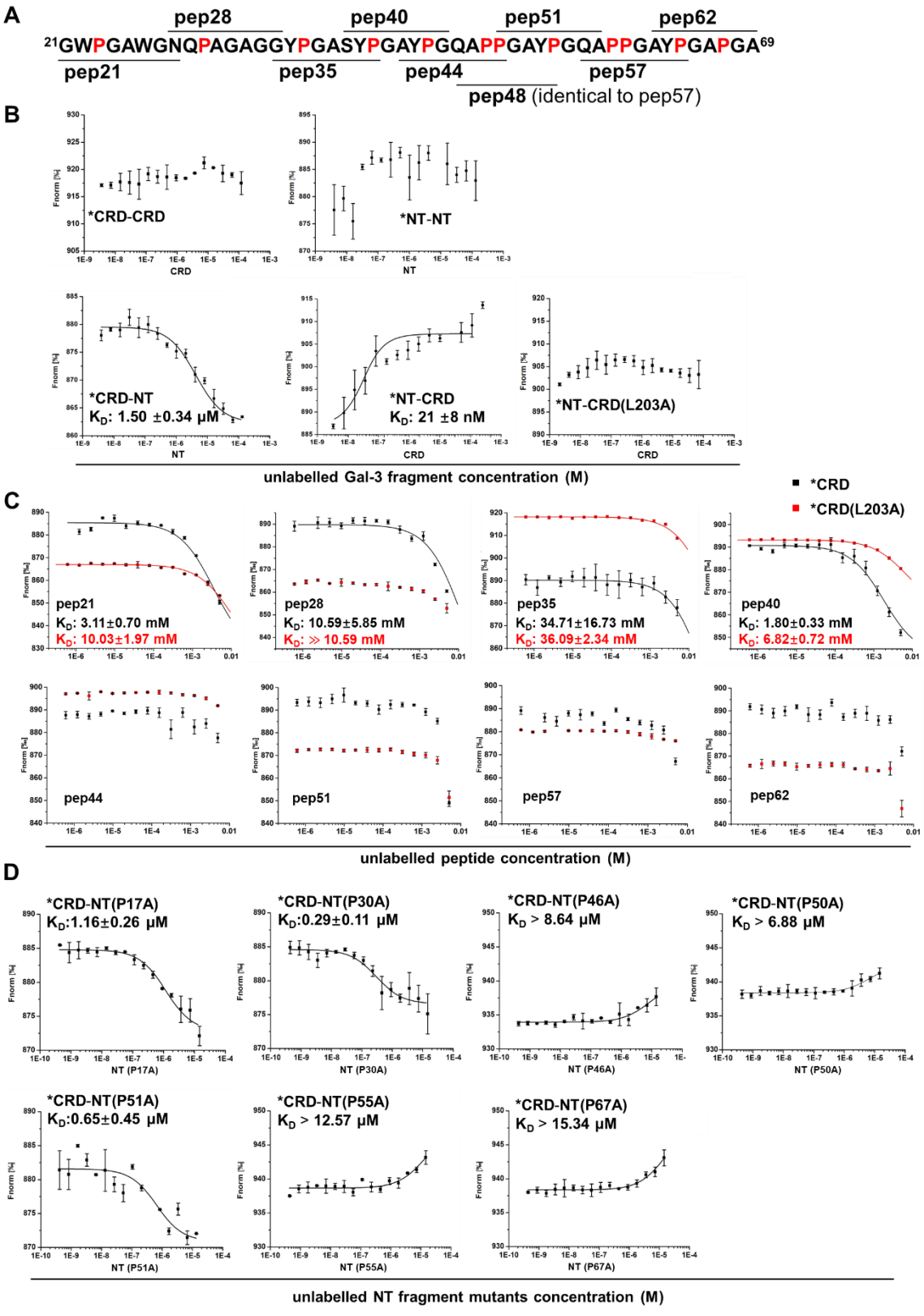
A
pep28
pep40
pep51
pep62
21GWPGAWGNQPAGAGGYPGASYPGAYPGQAPPGAYPGQAPPGAYPGAPGA69
pep21
pep35
pep44
pep57
pep48 (identical to pep57)
B
*CRD-CRD
*NT-NT
*CRD-NT
K_D: 1.50 ±0.34 µM
*NT-CRD
K_D: 21 ±8 nM
*NT-CRD(L203A)
Fnorm [‰]
CRD
NT
unlabelled Gal-3 fragment concentration (M)
C
*CRD
*CRD(L203A)
pep21
K_D: 3.11±0.70 mM
K_D: 10.03±1.97 mM
pep28
K_D: 10.59±5.85 mM
K_D: ≫ 10.59 mM
pep35
K_D: 34.71±16.73 mM
K_D: 36.09±2.34 mM
pep40
K_D: 1.80±0.33 mM
K_D: 6.82±0.72 mM
pep44
pep51
pep57
pep62
unlabelled peptide concentration (M)
D
*CRD-NT(P17A)
K_D:1.16±0.26 µM
*CRD-NT(P30A)
K_D:0.29±0.11 µM
*CRD-NT(P46A)
K_D > 8.64 µM
*CRD-NT(P50A)
K_D > 6.88 µM
*CRD-NT(P51A)
K_D:0.65±0.45 µM
*CRD-NT(P55A)
K_D > 12.57 µM
*CRD-NT(P67A)
K_D > 15.34 µM
NT (P17A)
NT (P30A)
NT (P46A)
NT (P50A)
NT (P51A)
NT (P55A)
NT (P67A)
unlabelled NT fragment mutants concentration (M)

Fig. S10. Prolines are involved in NT–CRD interactions. (*A*) Schematic diagram of the peptide sequence. NT octapeptides are termed pep21 to pep62, where the number indicates the position of the first amino acid residues in that particular peptide as labelled. Note that the pep48 sequence is identical to that of pep57. (*B-D*) Binding interactions were determined using the MST method. (*B*) Binding between CRDs was measured with 25 nM fluorescently labelled CRD (marked as *CRD) and the titration of unlabelled CRD up to 120 μM. NT–NT interactions were investigated in a similar fashion using 25 nM fluorescently labelled full-length NT peptide (marked as *NT) and the titration of unlabelled full-length NT peptide up to 120 μM. CRD-NT binding was measured either by the titration of *CRD with unlabelled NT or by the titration of *NT with unlabelled CRD. (*C*) For MST assessment of CRD or CRD(L203A) interactions with NT octapeptides, 25 nM *CRD or *CRD(L203A) was titrated with each of the unlabelled octapeptides. (*D*) Full-length NT fragment mutants (P17A, P30A, P46A, P50A, P51A, P55A, P67A) were assessed for CRD interactions by titration 25 nM *CRD with each unlabelled NT fragment. Data are shown as the mean ± SD (n=3).

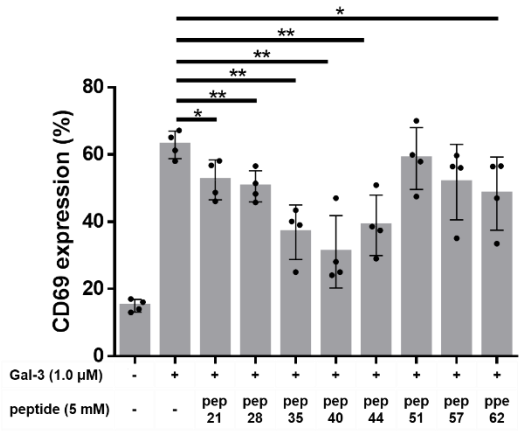

Fig. S11. Antagonizing effects of the octapeptides on Gal-3-induced T-cell activation. Jurkat cells were incubated with 1.0 μM Gal-3 in the presence or absence of peptides for 6 h, followed by the determination of CD69 expression by flow cytometry (data shown as the mean ± SD (n=4)). The *p* values were determined by Student's two-tailed *t*-test; $*p < 0.05$, $**p < 0.01$.

A

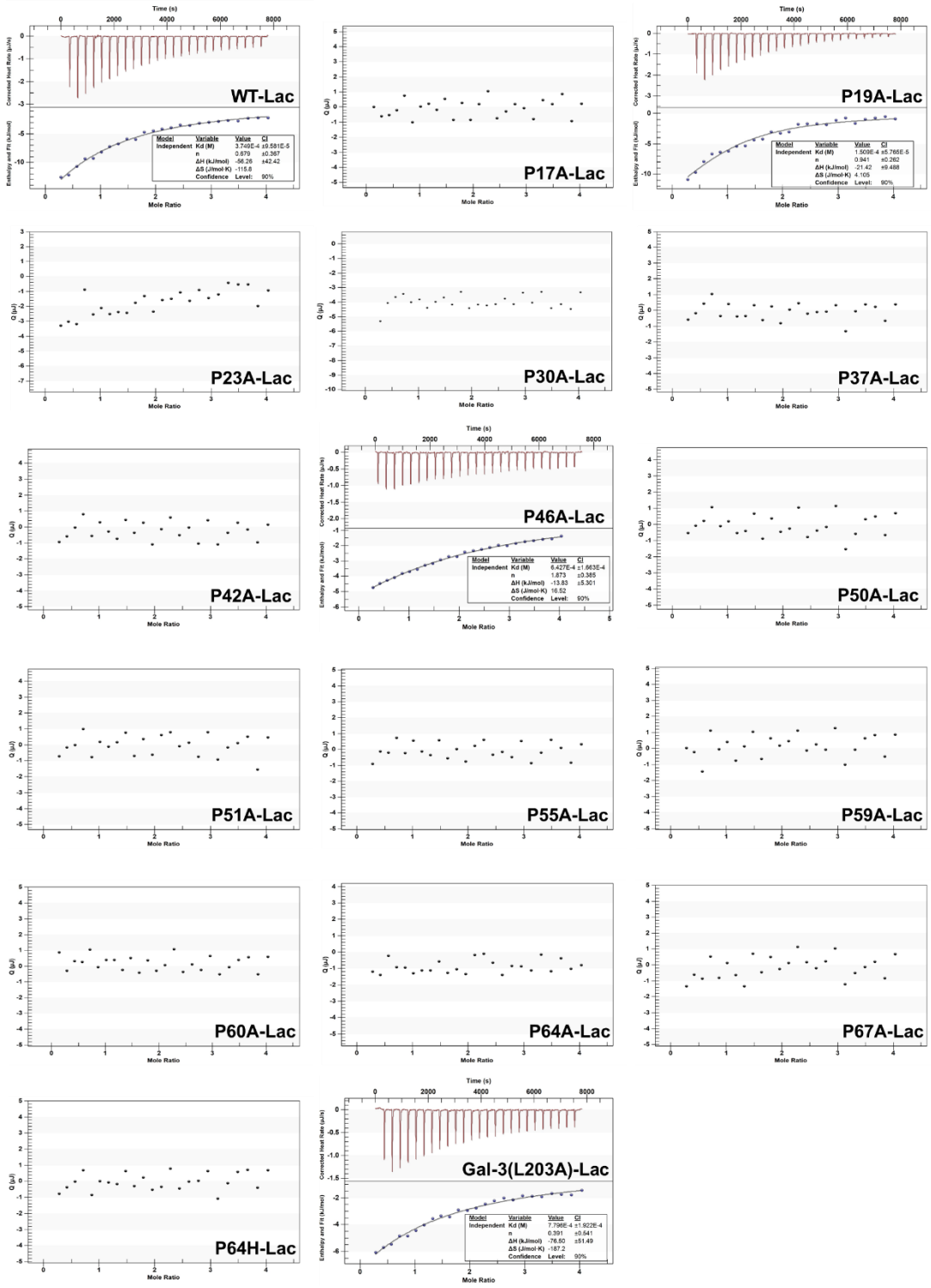
WT-Lac
P17A-Lac
P19A-Lac
P23A-Lac
P30A-Lac
P37A-Lac
P46A-Lac
P42A-Lac
P50A-Lac
P51A-Lac
P55A-Lac
P59A-Lac
P60A-Lac
P64A-Lac
P67A-Lac
P64H-Lac
Gal-3(L203A)-Lac
Time (s)
Mole Ratio

B

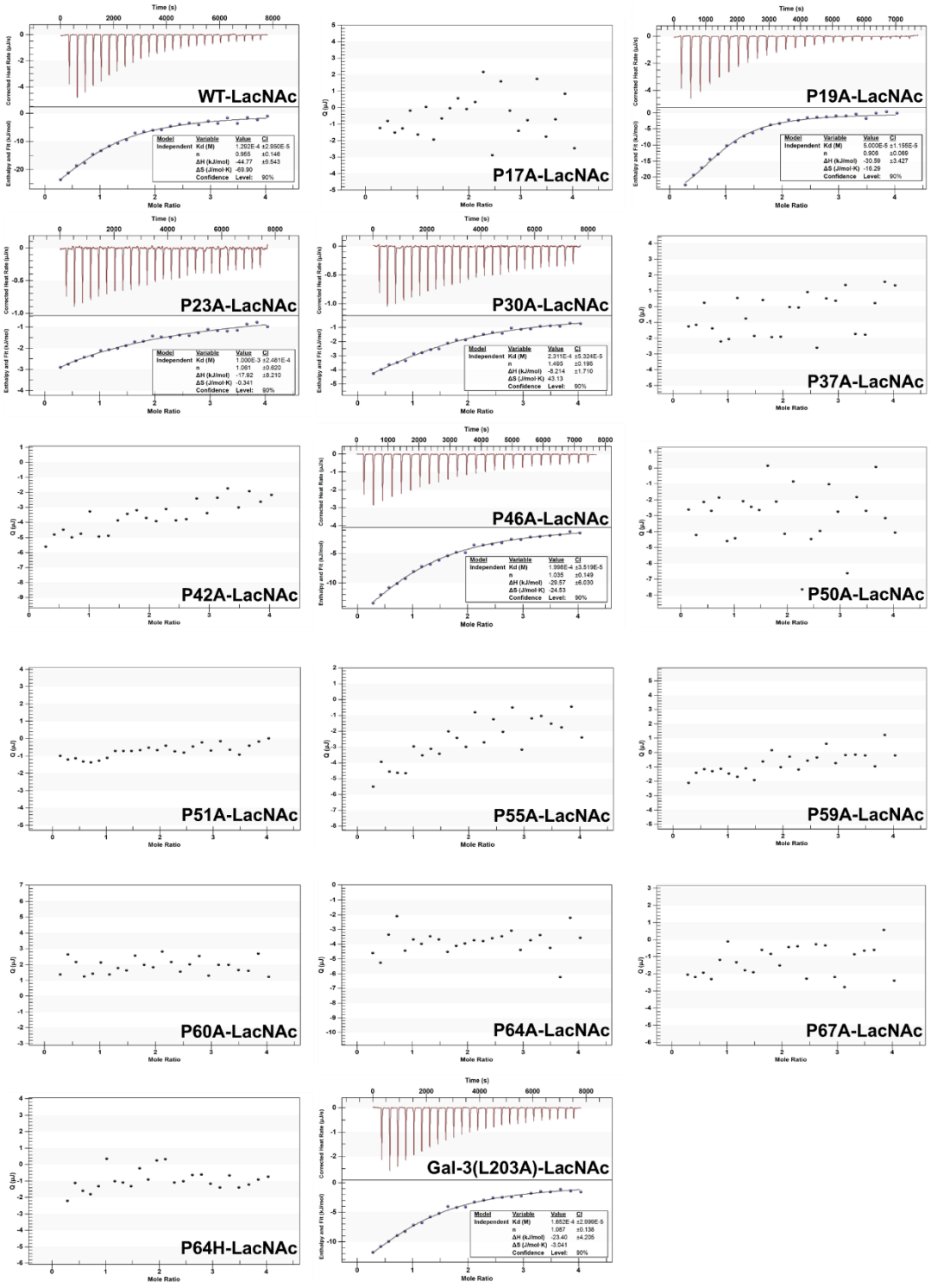
WT-LacNAc
P17A-LacNAc
P19A-LacNAc
P23A-LacNAc
P30A-LacNAc
P37A-LacNAc
P42A-LacNAc
P46A-LacNAc
P50A-LacNAc
P51A-LacNAc
P55A-LacNAc
P59A-LacNAc
P60A-LacNAc
P64A-LacNAc
P67A-LacNAc
P64H-LacNAc
Gal-3(L203A)-LacNAc
Time (s)
Corrected Heat Rate (µJ/s)
Enthalpy and Fit (kJ/mol)
Q (µJ)
Mole Ratio

C

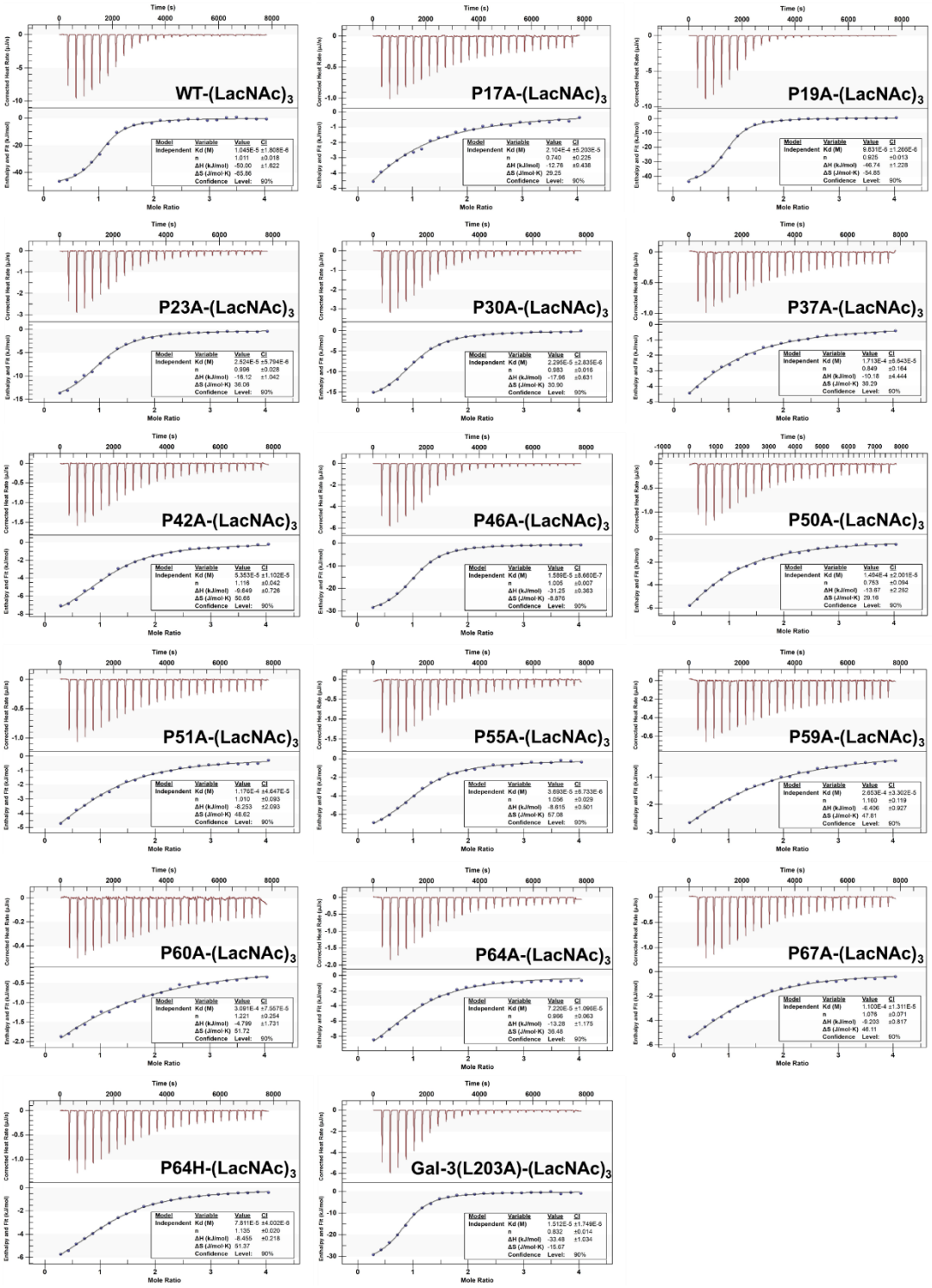

Fig. S12. Titration data of wild type (WT) Gal-3 and mutants binding to Lac (*A*), LacNAc (*B*), and (LacNAc)$_3$ (*C*). Related to Table 1.

A

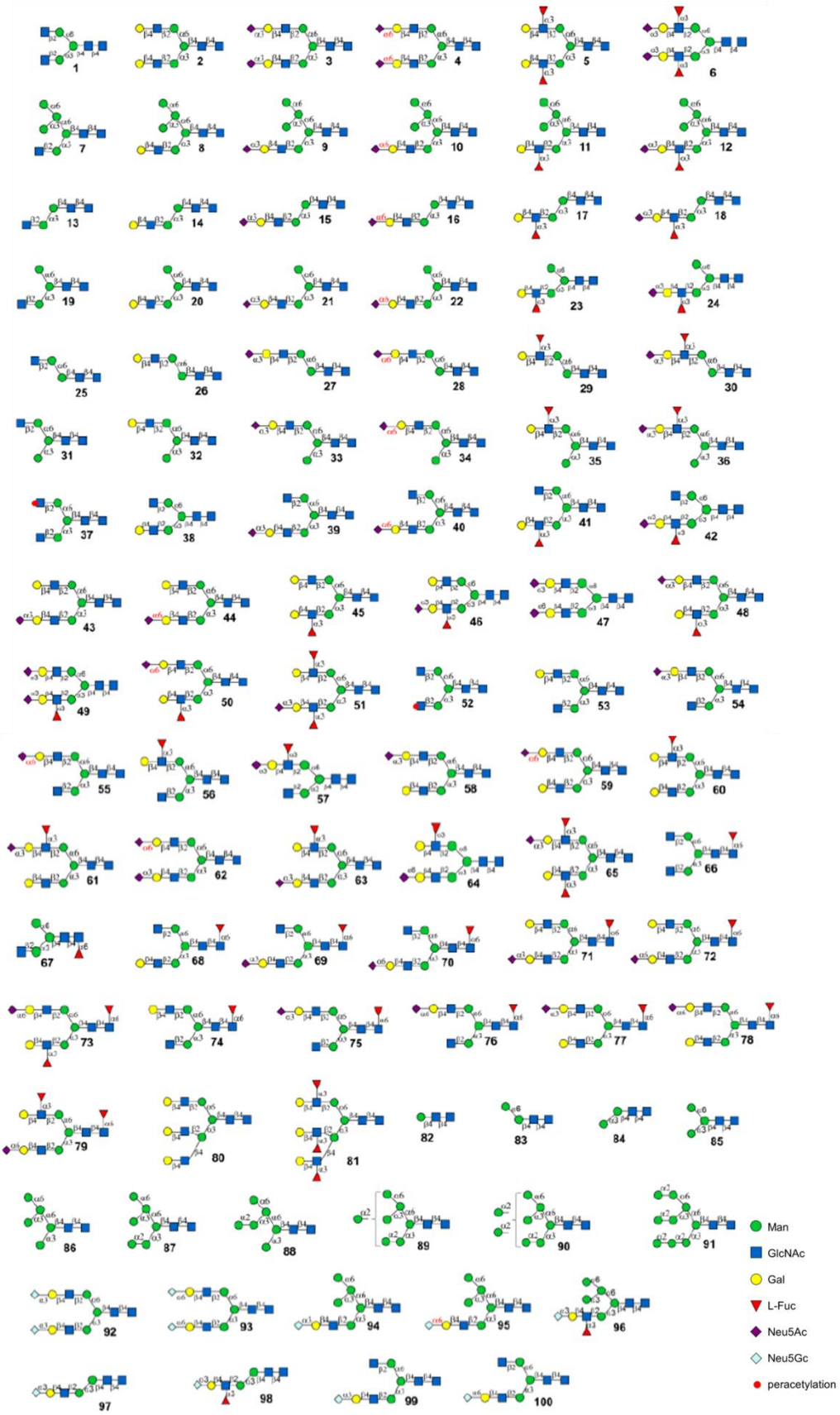
1
2
3
4
5
6
7
8
9
10
11
12
13
14
15
16
17
18
19
20
21
22
23
24
25
26
27
28
29
30
31
32
33
34
35
36
37
38
39
40
41
42
43
44
45
46
47
48
49
50
51
52
53
54
55
56
57
58
59
60
61
62
63
64
65
66
67
68
69
70
71
72
73
74
75
76
77
78
79
80
81
82
83
84
85
86
87
88
89
90
91
92
93
94
95
96
97
98
99
100
Man
GlcNAc
Gal
L-Fuc
Neu5Ac
Neu5Gc
peracetylation

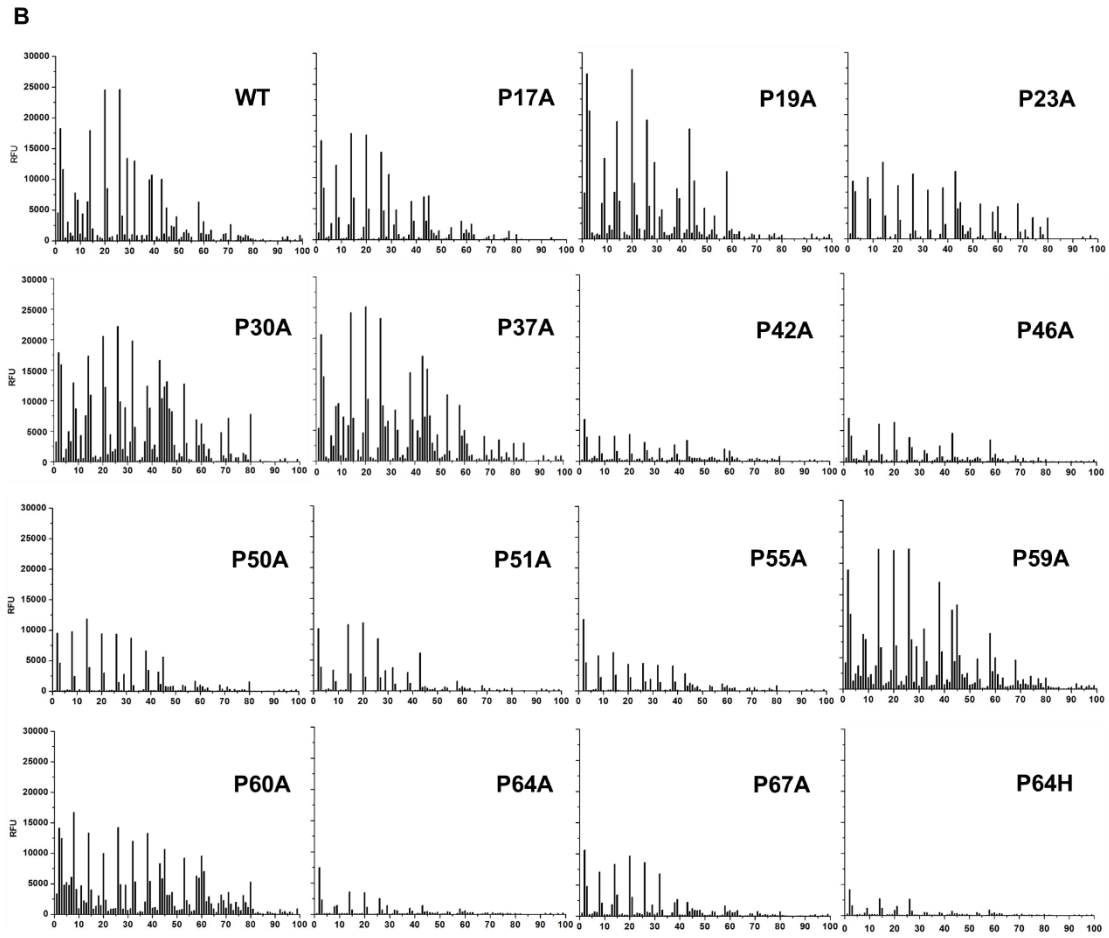

Fig. S13. Assessment of the effect of proline mutation on Gal-3 binding to glycans by using glycan arrays. (*A*) Sugar structures in the glycan array. (*B*) Binding profiles of WT Gal-3 and its mutants. The highest RFU values on the *y*-axis indicate which glycans bind most strongly to each NT proline mutant.

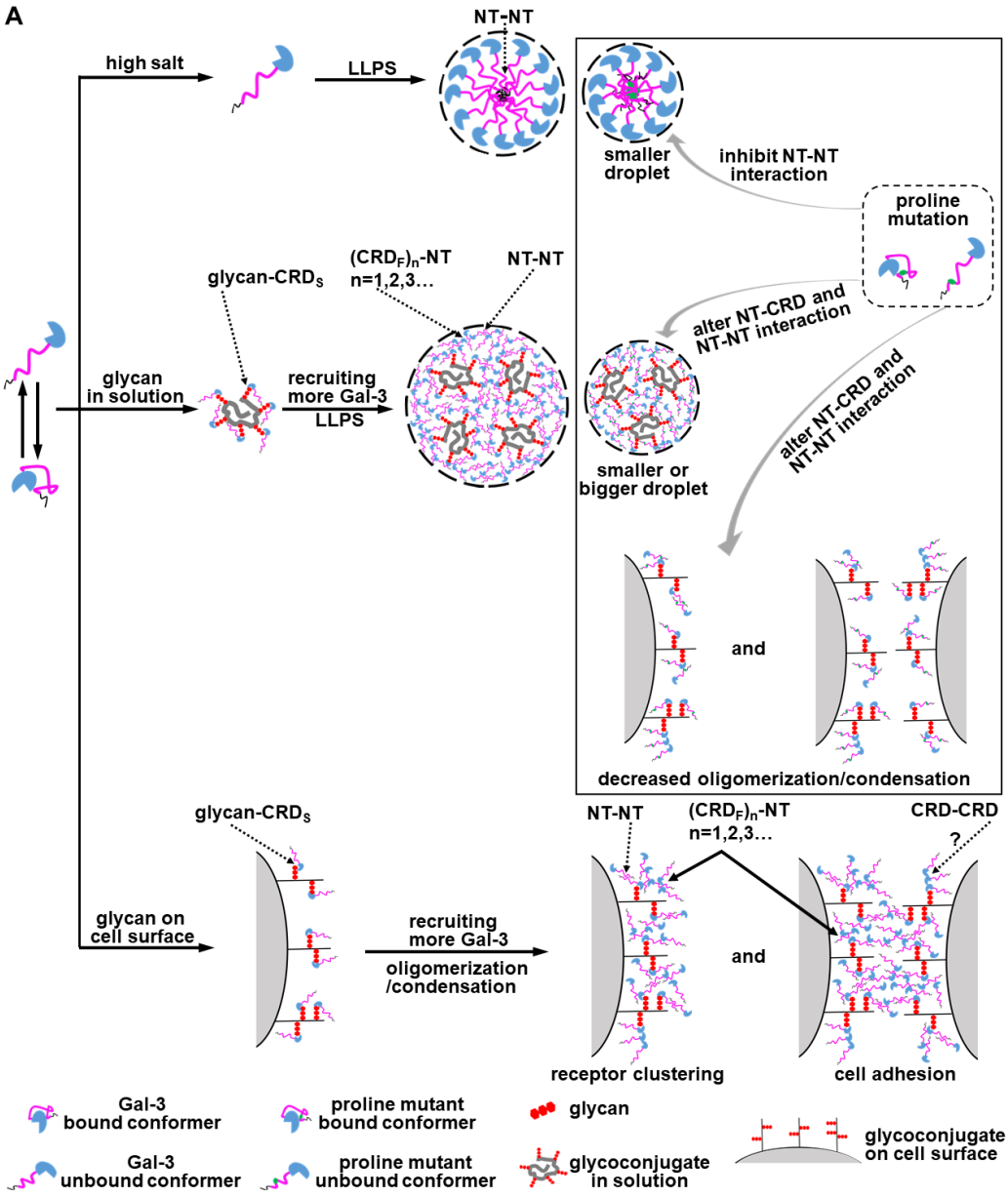

B

	Gal-3Δ12	Gal-3Δ68	CRD	NT
high salt	similar	no droplet	no droplet	similar
glycan in solution	similar	smaller	no droplet	no droplet
glycan on cell surface	—	decreased	decreased	no binding

comparison with full-length Gal-3

—, not detected.

Fig. S14. Model of Gal-3 oligomerization/phase separation. (*A*) Gal-3 oligomerization/phase separation under different conditions as presented in the Discussion. CRD_S, CRD S-face. CRD_F, CRD F-face. (*B*) Functions of different structural domains in Gal-3 oligomerization/phase separation as shown by comparison with full-length Gal-3.

Supplementary Tables

Table S1 Grey analysis of Gal-3 and CD146 in the sedimentation assay. Related to Fig. 2.

initial CD146:Gal-3	supernatant CD146 grey analysis	pellet CD146 grey analysis	pellet CD146 concentration	supernatant Gal-3 grey analysis	pellet Gal-3 grey analysis	pellet Gal-3 concentration	pellet CD146:Gal-3
200 nM:10 µM	1585	1131	83 nM	9034	2472	2.15 µM	1:26
200 nM:20 µM	1835	5654	151 nM	9681	5211	7.00 µM	1:46
200 nM:30 µM	1421	8995	173 nM	10356	5630	10.57 µM	1:61
200 nM:40 µM	1093	7621	175 nM	11008	5937	14.01 µM	1:80
200 nM:50 µM	847	7071	179 nM	12842	5291	14.59 µM	1:82

Table S2. HSQC Δδ and ΔINT for WT Gal-3 vs. NT proline mutants. Sequence-averaged values are shown. ΔINT (NT) is for the average value for the NT sequence alone.

NT mutant	Δδ (ppm)	ΔINT	ΔINT (NT)
P19A	0.0124	- 0.358	- 0.641
P23A	0.0176	- 0.057	- 0.126
P30A	0.0186	+0.086	+0.017
P37A	0.0193	- 0.113	- 0.017
P42A	0.0232	- 0.364	- 0.129
P46A	0.0664	- 0.109	- 0.051
P50A	0.0146	+0.066	+0.091
P51A	0.0079	- 0.142	- 0.305
P55A	0.0275	- 0.165	- 0.065
P59A	0.0186	- 0.016	- 0.072
P64A	0.0127	- 0.132	- 0.118
P67A	0.0125	- 0.169	- 0.287

Table S3 Summary of proline function. Related to Fig. 1, 5 and Table 1.

	P17A	P19A	P23A	P30A	P37A	P42A	P46A	P50A	P51A	P55A	P59A	P60A	P64A	P67A	P64H
HMEC-1 migration (Fig. 1*A*)	**-***	**-***	**-****	**-****	**-*****	**-****	**-****	**-****	**-****	**-******	**-****	**-*****	**-*****	**-*****	**-*****
Jurkat activation (Fig. 1 *B* and *C*)					**-****			**-****		**-****		**-****	**-***	**-***	**-***
Hemagglutination (Fig. 1*D*)					**-******			**-******	**-*****	**-***		**-******	**-****	**-***	**-****
Endocytosis (Fig. 1*E*)				**-****	**-***							**-****	**-***	**-****	**-***
High salt-induced LLPS (Fig. 5*A*)					**-***					**-****			**-****	**-***	**-****
CD146-induced LLPS (Fig. 5*B*)				**-******	**-*****				**-****	**-******	**-***		**-****	**-*****	**-****
CD45-induced LLPS (Fig. 5*C*)	**-******		**-****	**-****	**-******			**-***	**-******	**-******	**-******	**+*****	**+****	**-******	**+****
CD7-induced LLPS (Fig. 5*D*)	**-*****				**-*****				**-*****			**-*****	**+****	**-****	**+***
CD71-induced LLPS (Fig. 5*E*)	**-*****		**-*****	**-****	**-*****		**-****		**-****		**-***	**-***	**-****	**-****	**-****
Binding to Jurkat (Fig. 5*H*)								**-****	**-***	**-***		**-****	**-***	**-***	**nd**
Binding to HMEC-1 (Fig. 5*H*)			**+***					**-****	**-***	**-***		**-****	**-***	**-***	**nd**
Binding to Lac (Table 1)	##	#	##	##	##	##	#	##	##	##	##	##	##	##	##
Binding to LacNAc (Table 1)	##	#	##	#	##	##	#	##	##	##	##	##	##	##	##
Binding to $(LacNAc)_3$ (Table 1)	##		##	#	##	##	#	##	##	#	##	##	##	##	##
Binding to CD146 (Fig. 5 *F* and *G*)	#	#	#	#	##	#	#	##	#	##	#	##	#	##	**nd**

+, promotion; **-,** inhibition, nd, not detected. ***p* < 0.05; ****p* < 0.01; *****p* < 0.001; ******p* < 0.0001; #, proline mutation affected Gal-3 amount and/or Gal-3 affinity/avidity (or glycan footprints), ## > #.

SI References

1. X. Gao *et al.*, The two endocytic pathways mediated by the carbohydrate recognition domain and regulated by the collagen-like domain of galectin-3 in vascular endothelial cells. *PLoS One* **7**, e52430 (2012).
2. Y. Si *et al.*, Human galectin-2 interacts with carbohydrates and peptides non-classically: new insight from X-ray crystallography and hemagglutination. *Acta Bioch. Bioph. Sin.* **48**, 939-947 (2016).
3. E. Salomonsson *et al.*, Mutational tuning of galectin-3 specificity and biological function. *J. Biol. Chem.* **285**, 35079-35091 (2010).
4. Z. Zhang, Y. Zheng, H. Wang, Y. Zhou, G. Tai, CD146 interacts with galectin-3 to mediate endothelial cell migration. *Febs Lett.* **592**, 1817-1828 (2018).
5. X. Gao *et al.*, The Inhibitory effects of a rhamnogalacturonan I (RG-I) domain from ginseng pectin on galectin-3 and its structure-activity relationship. *J. Biol. Chem.* **288**, 33953-33965 (2013).
6. G. Levi, V. I. Teichberg, Isolation and physicochemical characterization of electrolectin, a beta-D-galactoside binding lectin from the electric organ of Electrophorus electricus. *J. Biol. Chem.* **256**, 5735-5740 (1981).
7. H. Ippel *et al.*, Intra- and intermolecular interactions of human galectin-3: assessment by full-assignment-based NMR. *Glycobiology* **26**, 888-903 (2016).
8. F. Delaglio *et al.*, NMRPipe: a multidimensional spectral processing system based on UNIX pipes. *J. Biomol. NMR* **6**, 277-293 (1995).
9. B. A. Johnson, R. A. Blevins, NMR View: A computer program for the visualization and analysis of NMR data. *J. Biomol. NMR* **4**, 603-614 (1994).
10. J. Seetharaman *et al.*, X-ray crystal structure of the human galectin-3 carbohydrate recognition domain at 2.1-A resolution. *J. Biol. Chem.* **273**, 13047-13052 (1998).